Mature microRNA-binding protein QKI promotes microRNA-mediated gene silencing

Kyung-Won Min[1,2,‡,*], Myung Hyun Jo[3,‡], Minsuk Song[3,‡], Seungbeom Ko[1], Ji Won Lee[2], Min Ji Shim[2], Kyungmin Kim[2], Hyun Bong Park[2], Shinwon Ha[4], Hyejin Mun[1], Ahsan Polash[5], Markus Hafner[5], Jung-Hyun Cho[1], Dong-San Kim[4], Sungchul Hohng[3], Sung-Ung Kang[4,*], Je-Hyun Yoon[1,6,*]

[1]Department of Biochemistry and Molecular Biology, Medical University of South Carolina, Charleston, SC 29425, USA

[2]Department of Biology, Gangneung-Wonju National University, Gangneung, 25457, Republic of Korea

[3]Department of Physics & Astronomy, Seoul National University, Seoul, 08826, Republic of Korea

[4]Neuroregeneration and Stem Cell Programs, Institute for Cell Engineering, Johns Hopkins University School of Medicine, Baltimore, MD 21205, USA

[5]Laboratory of Muscle Stem Cells and Gene Regulation, National Institute of Arthritis and Musculoskeletal and Skin Diseases, National Institutes of Health, Bethesda, MD 20892, USA

[6]Lead Contact

‡These authors equally contributed to this study.

*Corresponding authors: yoonje@musc.edu (J,-H.Y.), skang34@jhmi.edu (S.-U.K.), minkw@gwnu.ac.kr (K.-W.M.)

ABSTRACT

Although Argonaute (AGO) proteins have been the focus of microRNA (miRNA) studies, we observed AGO-free mature miRNAs directly interacting with RNA-binding proteins, implying the sophisticated nature of fine-tuning gene regulation by miRNAs. To investigate microRNA-binding proteins (miRBPs) globally, we analyzed PAR-CLIP data sets to identify RBP quaking (QKI) as a novel miRBP for let-7b. Potential existence of AGO-free miRNAs were further verified in genetically engineered AGO-depleted human and mouse cells. We have shown that QKI serves as an auxiliary factor empowering AGO2/let-7b-mediated gene silencing. Depletion of QKI decreases interaction of AGO2 with let-7b and target mRNA, consequently controlling target mRNA decay. QKI, however, also suppresses the dissociation of let-7b from AGO2, and slows assembly of AGO2/miRNA/target mRNA complexes at the single-molecule level. We also revealed that QKI suppresses cMYC expression at post-transcriptional level, and decreases proliferation and migration of HeLa cells, demonstrating that QKI is a tumor suppressor gene by in part augmenting let-7b activity. Our data show that QKI is a new type of RBP implicated in the versatile regulation of miRNA-mediated gene silencing.

KEYWORDS

QKI;   AGO2;   RNA-binding   protein;   let-7b

INTRODUCTION

Post-transcriptional gene regulation is a key mechanism for eukaryotic organisms, enabling them to respond rapidly to environmental changes by synthesizing proteins with proper timing and location (Gehring *et al*, 2017; Jackson *et al*, 2010; Jonas & Izaurralde, 2015). This regulatory mechanism is mainly governed by three major factors: RNA-binding proteins (RBPs), non-coding RNAs such as microRNAs (miRNAs), and long non-coding RNAs (lncRNAs) (Gehring *et al.*, 2017; Ha & Kim, 2014; Yoon *et al*, 2013a). Approximately 2,300 or higher number of miRNAs are expressed in human cells, which target complementary sequences in mRNAs and lncRNAs, to suppress mRNA translation or induce target RNA degradation (Alles *et al*, 2019; Chiang *et al*, 2010; Ha & Kim, 2014). The mechanism(s) of miRNA biogenesis and gene silencing have been well studied whereas miRNA decay occurs via terminal modification and target-directed miRNA degradation (Chatterjee & Großhans, 2009; Han *et al*, 2020; Shi *et al*, 2020; Towler *et al*, 2015).

In order for miRNAs to silence target mRNAs, mammalian cells require specialized proteins to promote target mRNA decay and suppress translation. Argonaute (AGO) proteins are direct binding partners of mature miRNAs, and central components of the RNA-induced Silencing Complex (RISC). DICER1 directly interacts with the AGOs and transfers a miRNA duplex to AGOs, with the thermodynamically favored guide strand being retained, and the passenger strand being discarded from the AGOs (Kawamata *et al*, 2009; Kim *et al*, 2016). The AGO-bound miRNAs then guide the AGOs to target mRNAs for decapping, deadenylation, and exo-ribonucleolytic decay (Fabian & Sonenberg, 2012).

Recently, miRNA's fate after AGO-mediated gene silencing has been explored using RNA labeling and high throughput RNA-seq analysis (Baccarini *et al*, 2011; Becker *et al*, 2019; Elbarbary *et al*, 2017; Ghini *et al*, 2018; Kingston & Bartel, 2019; Kleaveland *et al*, 2018; Marzi *et al*, 2016; Sheu-

65   Gruttadauria *et al*, 2019; Shukla *et al*, 2019). The most mature miRNAs are highly stable (Reichholf *et*

66   *al*, 2019) and are produced at rates as fast as 110 ± 50 copies/cell/min in mouse embryonic fibroblasts,

67   and miRNAs spanning a highly complementary target site are prone to be degraded for AGO2 recycling

68   since AGO2 outlives miRNAs (Kingston & Bartel, 2019). Decay of selective mature miRNAs is either

69   influenced by the 3'-end trimming of pre-miRNAs and mature miRNAs (Katoh *et al*, 2009; Lee *et al*,

70   2019; Li *et al*, 2005; Shukla *et al.*, 2019) or by proteasome-dependent turnover of AGO2 when miRNA-

71   mRNA interacts via extensive base paring (Han *et al.*, 2020; Shi *et al.*, 2020).

72   In this study, our findings suggest that several types of RBPs, including quaking (QKI), directly

73   bind a subset of mature miRNAs. QKI was previously implicated in mRNA splicing, export, and decay

74   (De Bruin *et al*, 2016; Larocque *et al*, 2002; Thangaraj *et al*, 2017) and circular RNA biogenesis (Conn

75   *et al*, 2015). Specifically, our observations indicated that QKI: (i) directly binds a subset of mature

76   miRNAs, (ii) promotes the interaction of AGO2 with let-7b, (iii) decreases the stability of mRNA

77   targeted by let-7b, (iv) inhibits the dissociation of let-7b from AGO2, and (v) delays the kinetics of

78   AGO2/miRNA/target mRNA complex assembly at a single-molecular level. Furthermore, our results

79   also suggest that QKI imparts anti-tumorigenic effects partly by enhancing AGO2/let-7b/*cMYC* axis.

80   Here, we reveal newly identified QKI as a novel miRNA binding protein and add an additional layer of

81   complexity in miRNA-mediated gene silencing.

82   **RESULTS**

83   *Canonical RBPs directly bind mature miRNAs, which are free of AGO proteins*

84   In order to profile RBPs directly binding with mature miRNAs, we first analyzed the published

85   CLIP data sets (2075 in total) and then searched RBPs (311 in total) cross-linked with mature miRNA

86   let-7 family, miR-21, and miR-130b (Zhu *et al*, 2019). Since Photoactivatable Ribonucleoside-Enhanced

87   Crosslinking and Immunoprecipitation (PAR-CLIP) data provides the most reliable measure of RBP and

88   RNA crosslinking based on T-to-C conversion (Hafner *et al*, 2010), we plotted genomic coordinates of

89   let-7a-1, let-7b, let-7c (**Figure 1 and Table S1**), let-7a-2, let-7a-3, let-7d (**Figure S1 and Table S1**),

90   miR-21 and miR-130b (**Figure S2 and Table S1**) corresponding to their mature miRNA sequences. We

91   chose those miRNAs as candidates because they are well-characterized in cellular processes and human

92   diseases (Büssing *et al*, 2008; Massey *et al*, 2018; Sheedy, 2015; Wang *et al*, 2010b; Yamamichi *et al*,

93   2009; Zhang *et al*, 2016). Our analysis revealed 7 RBPs binding with mature let-7a-1 (**Figure 1A**), 36

94   RBPs with let-7b (**Figure 1B**), 29 RBPs with let-7c (**Figure 1C**), 16 RBPs with let-7d (**Figure S1B**), 87

95   RBPs with miR-21 (**Figure S2A**), and 37 RBPs with miR-130b (**Figure S2B**). T-to-C conversion ratio

96   also indicates that the binding with RBPs and mature miRNA is comparable to AGO binding (**Figure 1**

97   **and Figure S1-S2**). Common RBPs binding with let-7, miR-21 and miR-130b include AGO, HuR,

98   AUF1 and QKI (**Figure S1C and S2C**). These results demonstrate that there is a pool of RBPs directly

99   binding with mature miRNAs.

100   MiRNAs are processed by DROSHA and DICER, and then loaded directly to AGO proteins

101   (Gregory *et al*, 2004; Hafner *et al.*, 2010; Lee *et al*, 2003). There are many reports that mature miRNAs

102   generally are degraded rapidly after dissociation with AGOs (Kingston & Bartel, 2019; Reichholf *et al.*,

103   2019). Since our findings in **Figure 1** demonstrated that many RBPs directly bind with mature miRNAs,

104   one possibility is that there is a pool of mature miRNAs resistant to degradation after dissociation from

105 AGO proteins. To prove this idea, we set up the assay of AGO immunodepletion using antibodies

106 recognizing AGO2 or Pan-AGO proteins. After series of immunoprecipitation using human HeLa cells

107 and mouse embryonic fibroblasts (MEFs) (**Figure 2A and 2B**), we measured amount of let-7b, miR-21,

108 and miR-130b from total RNAs or supernatants after the third immunoprecipitation. Our RNA-seq data

109 revealed that ~10% of mature let-7b, let-7i and miR-21 still exist in the lysates after immunodepletion of

110 AGO2 and Pan-AGO in human cells (**Figure 2C and Table S2**). However, let-7c, let-7e, and miR-130b

111 were depleted in the supernatant after the third immunoprecipitation suggesting that they are quickly

112 degraded after dissociation from AGO proteins (**Figure 2C**). In contrast, mature miRNAs from MEFs

113 are still observed after AGO2 or Pan-AGO depletion (~10%) indicating that mouse cells contain more

114 mature miRNAs free of AGO proteins (**Figure 2D and Table S2**). These results indicate that a subset of

115 mature miRNAs exist in the form of AGO-free complex.

116 Genetic deletion of either AGO1 or AGO2 as well as double deletion marginally affects level of

117 mature let-7b both in miRNA counting and RNA-seq (**Figure S3A**). Triple knockout of AGO1, 2 and 3

118 in HCT116 cells (AGO TKO) also revealed that there is still significant amount of mature let-7b, miR-

119 21, miR-100, and let-7i even when there are no AGO proteins (**Figure 2E *Right* and Table S2**). RNA-

120 seq data also supported our findings that genetic deletion of AGO1, 2, and 3 did not affect mature

121 miRNA level globally (**Figure 2F**) as observed in *Dicer* and *Drosha* knockout (Ruby *et al*, 2007; Yang

122 *et al*, 2010). Although the expression of passenger strand increased in AGO TKO cells, the mature

123 strands were predominantly expressed in AGO TKO cells (**Figure S3B and Table S2**). We also

124 confirmed that comparable let-7b copy numbers are presented in AGO TKO cells compared with WT

125 using AGO-FISH assay (**Figure 2G**). In MEFs, level of let-7b was resistant to deletion of AGO2 both in

126 RNA-seq and miRNA counting (**Figure 2D and Figure S3C**), and even the stability of miRNAs did not

127 change significantly (**Figure S3D**). These findings demonstrate that there are a portion of mature

128   miRNAs which are not associated with AGO proteins and suggest that there should be distinct function

129   of RBPs directly binding with mature miRNAs.

130

131   *QKI enhances interaction of AGO2 with let-7b*

132   Since our results showed that QKI is associated with let-7 family (**Figure S1C**)**,** we thereafter

133   focused on let-7b, mainly due to its known functions in normal physiology and pathogenesis such as

134   cancer, for investigating QKI's role in miRNA function. Direct interaction of QKI and let-7b predicts

135   competition of QKI with AGO2 for let-7b binding (**Figure 3A**). To test this hypothesis, we depleted

136   QKI in HeLa cells and, using Ribonucleoprotein Immunoprecipitation (RIP) RT-qPCR analysis,

137   determined how this depletion affects the interaction of AGO2 with let-7b. Our analysis showed that

138   depletion of QKI by short hairpin RNA (shRNA) significantly decreased the abundance of let-7b in

139   AGO2 immunoprecipitates without affecting the expression of let-7b (**Figure 3B**). These results suggest

140   that QKI promotes interaction of AGO2 and let-7b in HeLa cells.

141   To address how QKI facilitates assembly of AGO2-let-7b complexes, we investigated miRNA

142   transfer (**Figure 3C**) by performing the single-molecule AGO2 protein-miRNA binding assay as we

143   reported previously (Yoon *et al*, 2015). To observe let-7b loading onto AGO2 in real-time, recombinant

144   human AGO2 proteins were immobilized on a PEG-passivated and biotin-functionalized surface using

145   an anti-His tag antibody (**Figure 3D**). Cy5-labeled let-7b (200 pM) was injected with or without

146   recombinant QKI (100 nM) and the appearance of let-7b fluorescence signals were monitored. Even

147   when let-7b was pre-bound to QKI, we observed loading, showing that the let-7b can be transferred

148   from QKI to AGO2. The let-7b loading rate with QKI (**Figure 3E-H**) was slower than that with AUF1

149   previously reported (Yoon *et al.*, 2015). These findings suggest that QKI facilitates the assembly of

150   AGO2-let-7b in cells by directly transferring let-7b to AGO2. It also implicates that transient formation

151 of a QKI:AGO2:let-7b ternary complex slows both on- and off-rates of miRNA. If the effect of QKI on

152 the let-7b off-rate is significantly more than on the let-7b on-rate, the steady-state equilibrium would be

153 pushed in favor of the let-7b-bound complex, as reflected in the RIP data. (**Figure 3B, and see**

154 **discussion**).

155

156 ***QKI promotes decay of let-7 target mRNAs***

157 Next, we tested the consequence of QKI's regulation of AGO2 binding to let-7b on target mRNA

158 decay. We compared enrichment of a let-7b target mRNA, *POLR2D* mRNA, as predicted in TargetScan

159 and in our previous study (Yoon *et al.*, 2015) on AGO2 immunoprecipitates when we transfected control

160 or QKI shRNA in HeLa cells. Similar to the enrichment of let-7b on AGO2, the depletion of QKI

161 decreased enrichment of *POLR2D* mRNA on AGO2 (**Figure 4A *Left***). The QKI effects on interaction

162 of AGO2 and *POLR2D* mRNA inversely correlate on *POLR2D* mRNA steady-state levels (**Figure 4A**

163 ***Right***), possibly due to changes of *POLR2D* mRNA stability but not changes in AGO2 level (**Figure**

164 **4B**). To measure the stability of *POLR2D* mRNA after knocking down QKI (or luciferase as a control),

165 *POLR2D* and *GAPDH* mRNA were measured at select times (0, 2, 4, 6, and 8 hours) after treatment

166 with Actinomycin D. We observed that the stability of *POLR2D* mRNA increases as the half-life of

167 *POLR2D* mRNA ($t_{1/2,}$ 50% of original abundance) increases from 4.2 hours to 7.8 hours after silencing

168 of QKI in HeLa cells (**Figure 4C**). In contrast, the stability of *GAPDH* mRNA, (the house-keeping

169 mRNA), does not change.

170 We further compared the stability of luciferase reporter mRNA containing the 3' UTR of

171 *POLR2D* mRNA (Yoon *et al.*, 2015) in HeLa cells transfected with control or QKI shRNA. While the

172 half-life of the Firefly luciferase reporter mRNA increases from 4.5 hours to 9.2 hours with transfection

173 of QKI shRNA, the half-life of mutant reporter mRNA lacking the let-7b seed-sequence was resistant to

174   lowering QKI levels ($t_{1/2}$ = 5.0 hours) (**Figure 4D**). As an additional control, we examined *GAPDH*

175   mRNA, the stability of which did not change significantly. Overexpression of QKI increased the

176   enrichment of *POLR2D* mRNA on AGO2 (**Figure 4E *Left***) and decreased steady state level of *POLR2D*

177   mRNA (**Figure 4E *Right***) without changes of AGO2 level or immunoprecipitation efficiency (**Figure**

178   **4F**). To further investigate QKI's role in miRNA-mediated gene silencing, we generated a luciferase

179   reporter with *cMYC* 3' UTR spanning let-7b binding sites as predicted in mirTarBase database to

180   confirm the influence of QKI on let-7b activity. We cloned the full-length and minimum containing let-

181   7b binding sites of *cMYC* 3' UTR into a dual luciferase reporter construct and then co-transfected these

182   plasmids with either QKI or control plasmid into HeLa cells. QKI overexpression indeed decreased the

183   luciferase activity which is regulated by *cMYC* 3' UTR, indicating that QKI promotes let-7b-mediated

184   gene silencing (**Figure S4A**). We also observed downregulation of cMYC expression by western blot

185   analysis after QKI overexpression (**Figure S4B**). cMYC is associated with tumor progression involving

186   in cell proliferation and migration (Dang, 2012; Meškytė *et al*, 2020). Given that QKI suppresses cMYC

187   expression, we further investigated the impact of QKI on cell proliferation and migration.

188   Overexpression of QKI decreased proliferation and migration of HeLa cells (**Figure S4C and S4D**).

189   These results demonstrate that QKI suppresses cell proliferation and migration by enhancing let-7b-

190   mediated gene silencing.

191   A previous study reported that QKI is immunoprecipitated with AGO2 and C-terminal domain of

192   QKI is responsible for interaction with AGO2 in human cell lines (Wang *et al*, 2010a). To test whether

193   increased let-7b activity by QKI was due to the interaction between AGO2 and C-terminal domain of

194   QKI, we constructed Myc-tagged C-terminal truncated QKI (**Figure 5A, *Left***) and performed

195   immunoprecpitation using anti-Myc or anti-AGO2 antibodies followed by RT-qPCR in QKI-depleted

196   cells. Our data revealed that exogenous QKI can be associated with let-7b, but not QKI mutant lacking

197   C-terminal domain, suggesting that C-terminal domain may be required for interaction with let-7b

198   (**Figure 5A, *Middle***). AGO2 RIP also showed the restoration of let-7b enrichment on AGO2

199   immunoprecipitates when wild-type QKI is reintroduced compared to C-terminal mutant QKI (**Figure**

200   **5A, *Right***). We confirmed steady state levels of let-7b were not changed significantly suggesting that

201   QKI may neither influence miRNA biogenesis nor miRNA stability (**Figure 5B**). Consistently,

202   increased of *POLR2D* mRNA stability by QKI depletion was decreased by re-introduction of wild type

203   QKI but not by QKI- C-terminal truncated mutant (**Figure 5C**). The results demonstrate that interaction

204   of QKI with AGO2 could be important for transferring miRNAs which subsequently enhances target

205   RNA decay. Additionally, overexpression of AGO2 in QKI-depleted cells decreased stability of

206   *POLR2D* mRNA (**Figure 5D**) without affecting level of QKI proteins (**Figure 5E**), indicating that QKI-

207   mediated *POLR2D* mRNA decay is dependent on miRNA function. These results demonstrate that QKI

208   promotes decay of let-7b target mRNAs indirectly by transferring let-7b to AGO2. The latter action may

209   be achieved through multiple mechanisms: decapping, deadenylation, or endonucleolytic cleavage, and

210   further studies are needed to fully confirm and specify their role in the degradation.

211

212   ***QKI suppresses assembly of AGO2-let-7b-target mRNA complex, and dissociation of let-7b from***

213   ***AGO2.***

214   Possible mechanisms by which QKI promotes target mRNA decay are to accelerate assembly of

215   the AGO2-let-7b-target mRNA complex, and to inhibit release of miRNA from AGO2. We next

216   performed *in vitro* miRNA release assay whether QKI can repress dissociation of let-7b from AGO2

217   (Min *et al*, 2020). We incubated recombinant AGO2 (20 nM) with let-7b (20 pM), followed by

218   immunoprecipitation of AGO2, and the removal of free AGO2 after several washing steps. We then

219   compared the amount of let-7b from the supernatant after incubation of AGO2-let7b complex, in the

220   presence and absence of recombinant QKI (**Figure 6A**). Our RT-qPCR of let-7b revealed that the

221   addition of recombinant QKI significantly suppresses let-7b dissociation from AGO2. Similarly, we

222   observed suppression of let-7b and *POLR2D* mRNA release from AGO2 immunopellets by recombinant

223   QKI using HeLa cell lysates (**Figure 6B**). These results demonstrate that QKI maintains the interaction

224   of AGO2 and let-7b. In order to further substantiate our hypothesis which is that QKI promotes let-7b

225   mediated target gene silencing, we performed proximity ligation followed by PCR using HeLa cell

226   lysates (Broughton *et al*, 2016). In this assay, we crosslinked AGO2/let-7b/target RNA complexes using

227   UV-C light, digested protein-unbound RNA for internal ligating let-7b with target RNA fragment, and

228   then immunoprecipitated AGO2. After immunoprecipitation, intermolecular ligation step was performed

229   to ligate let-7b with their target RNAs. Let-7b-*POLR2D* mRNA chimeric RNA fragment were

230   subsequently converted to cDNA, and then relative amount were compared between control and QKI-

231   depleted HeLa cells (**Figure S5A**). As expected, we observed that depletion of QKI decreases the

232   amount of let-7b-*POLR2D* chimeric product bound to AGO2, indicating that QKI stabilizes let-7b and

233   *POLR2D* mRNA interaction (**Figure S5B**). Moreover, we also profiled total RNA and focused on

234   changes in let-7b target RNAs from control and QKI-depleted HeLa cells. The result showed that let-7b

235   target RNAs are prone to more presence when QKI is depleted (**Figure S5C**). These findings show that

236   QKI inhibits release of let-7b, and targets mRNA from the AGO2-containing gene-silencing complex.

237   Next, we tested if QKI affects assembly of AGO2-let-7b-target mRNA complex at the single-

238   molecule level, as performed previously (Jo *et al*, 2015; Min *et al*, 2017). We immobilized the fragment

239   of *POLR2D* 3' UTR containing the let-7b target sequence (**Figure 6D**), through a streptavidin–biotin

240   interaction. The 5' end of the target RNA was labeled with Cy3 to induce high FRET (Fluorescence

241   Resonance Energy Transfer) when Cy5-labeled let-7b is bound on the target RNA. The Cy5-labeled let-

242   7b was pre-incubated with an excess of AGO2 (25X, 1 μM), and the diluted reaction mixture (2 nM)

243   was injected into the detection chamber (**Figure 6E**). In this setting, the simultaneous appearance of

244   high FRET for Cy3 excitation, and the resulting Cy5 signal, indicates the binding of the RISC on target

245   RNA. The binding rate was measured by collecting the time delay between the solution injection and

246   high FRET signal from the binding events. Our results revealed that the assembly of AGO2-let-7b-

247   *POLR2D* fragment complex significantly slowed down about five times when recombinant QKI was

248   added (100 nM) over the indicated times (**Figure 6F-H**). The *in vitro* kinetic assay showed that QKI

249   significantly slows down the assembly of this complex, and suggest that QKI suppresses the kinetics of

250   AGO2-let-7b-target mRNA assembly.

251

252 **DISCUSSION**

253   MiRNAs and RBPs, including miRBPs, are key regulators of post-transcriptional gene

254 expression (Ciafrè & Galardi, 2013; Jonas & Izaurralde, 2015; Min *et al.*, 2017). Dysregulation of

255 miRNA target recognition, miRNA biogenesis, and their subcellular localization, alters cellular

256 physiology, and drives human pathologies such as cancer, inflammation, cardiac abnormalities,

257 ischemia/stroke, and neuronal degeneration (Abe & Bonini, 2013; Chen *et al*, 2017; Ding *et al*, 2011;

258 Rupaimoole *et al*, 2016; Zangari *et al*, 2017). Thus, investigation of interplay between miRNAs and

259 miRBPs will contribute to find clues to treat human diseases by targeting either miRNAs or miRBPs.

260   Although QKI has been studied by splicing of precursor mRNA in nucleus (Wu *et al*, 2002),

261 none of the previous studies reported QKI as a mature miRNA-binding protein. Our new findings show

262 that QKI binds directly to let-7b miRNA, and accelerates AGO2/let-7b-mediated target mRNA decay

263 (**Figure 1 and 4**). We also revealed that QKI acts as a tumor suppressor gene by partially increasing the

264 activity of let-7b in HeLa cells (**Figure S4**). QKI may empower miRNA-mediated gene silencing when

265 QKI expression or cytoplasmic localization changes. We do not know the exact molecular mechanisms

266 by which QKI decreases the stability of let-7b target mRNA, because QKI transfer of let-7b to AGO2:

267 (i) is inefficient (**Figure 3**), (ii) suppresses the kinetic assembly of AGO2/let-7b/*POLR2D* mRNA at the

268 single-molecule level, and (iii) inhibits disassembly of AGO2/let-7b/*POLR2D* mRNA complex (**Figure

269 6**). Even though we confirmed through chimera PCR in cell lysates that QKI is critical for let-7b and

270 *POLR2D* mRNA interaction (**Figure S5**), the detailed mechanistic function by which QKI stabilizes

271 AGO2/let-7b/target RNA remains to be determined.

272

273 ***Presence of mature miRNA without RISC assembly and novel miRBPs in addition to AGO-family***

274 ***proteins***

275   Mature miRNAs function in mRNA decay and translation as a part of RISC (Misiewicz-

276   Krzeminska *et al*, 2019). It has been reported that miRNAs dissociated from AGO are rapidly degraded

277   by mechanisms of Target-Directed MicroRNA Degradation (TDMD) (Han *et al.*, 2020; Kingston & Bartel,

278   2021; Kleaveland *et al.*, 2018; Shi *et al.*, 2020). Previous studies also revealed that levels of a subset of

279   mature miRNAs correlate with levels of Argonaute proteins (Diederichs *et al*, 2008; Martinez &

280   Gregory, 2013; O'Carroll *et al*, 2007; Reichholf *et al.*, 2019). However, our data showed that the

281   presence of AGO-free mature miRNAs existed in cytoplasm, which is supported by using RNA-seq of

282   AGO TKO cells data and AGO IP data. It indicated that there are other RBPs binding with mature

283   miRNA. Certain RBPs interact with mature miRNAs directly at high affinity (Zealy *et al*, 2017);

284   however, it is not known if these miRBPs also interact with duplex miRNAs. The results of our PAR-

285   CLIP analysis revealed a subset of mature miRNA as QKI targets (**Figure S1D**), not passenger strands.

286   Differences in amino acid sequences and structures between QKI and AGO proteins also suggest that

287   these two miRBPs have different modes of miRNA interactions, such as recognition of 5' phosphoryl

288   and 3' hydroxyl groups. It is also possible that miRBPs modulate miRNA-mediated gene silencing by

289   functioning as auxiliary factors surveilling target recognition by AGO proteins (Min *et al.*, 2017; Yoon

290   *et al*, 2013b), or simply compete with AGO proteins for miRNAs (Eiring *et al*, 2010). k_a of recombinant

291   QKI for let-7b (3.24×10^4 $M^{-1}s^{-1}$) slower than a wide range of eukaryotic proteins (Gleitsman *et al*, 2017)

292   but several proteins indeed exhibit k_{on} in a similar range of k_a for QKI with let-7b (Arluison *et al*, 1999;

293   Chen *et al*, 2005; Park-Lee *et al*, 2003; Park *et al*, 2000; Salomon *et al*, 2015; Shen & Shan, 2010).

294   Although we cannot exclude the possibility that QKI may not facilitate the direct loading of let-7b to AGO2,

295   other components would be necessary to facilitate the direct loading of let-7b to QKI, or that the transfer is

296   not very efficient. Further studies are needed to identify common sequences and, or structural motifs

297   among miRBPs to allow their interaction with mature miRNAs such as let-7b.

298

Mechanisms of miRNA-mediated gene silencing via delay of RISC assembly and disassembly

300   The discrepancy between results of cell-based biochemistry and single-molecule biophysics

301 suggests that there should be additional factors contributing to efficient RISC assembly, such as

302 scaffolding proteins supporting QKI and AGO2 interaction in specific locations (Wang *et al.*, 2010a). A

303 recent study argues that the AGO2 phosphorylation cycle regulates the interaction of AGO2 with target

304 mRNAs, to maintain the global efficiency of miRNA-mediated gene silencing (Golden *et al*, 2017). The

305 former study (Golden *et al.*, 2017) identified a protein kinase (CSNK1A1) and a phosphatase complex

306 (ANKRD52-PPP6C) involved in the hierarchical cycle of AGO2 phosphorylation. AGO2

307 phosphorylation could induce active disassembly of AGO2 and target mRNA complexes, giving rise to

308 increase availability of AGO to silence additional targets. Considering this, the kinetic repression of

309 AGO2-miRNA-target mRNA assembly by QKI *in vitro* (**Figure 6**) could promote mRNA decay in

310 mammalian cells. Future studies could investigate whether QKI influences AGO2 phosphorylation by

311 interacting with the aforementioned kinase and phosphatase complex, and/or regulating target mRNA

312 silencing.

313   In summary, our findings add growing evidence that novel miRBPs occupy AGO2-free mature

314 miRNAs functioning in miRNA metabolism. Our observations emphasize the regulation of

315 AGO2/miRNA/target mRNA assembly by QKI, which can impact upon target gene silencing. Our study

316 provides an insight upon how miRNA-binding activity of QKI is linked to cellular processes impacting

317 miRNA metabolism.

318 **METERIALS and METHODS**

319

320 **Contact for Reagent and Resource Sharing**

321 Further information and requests for resources and reagents should be directed to and will be fulfilled

322 by the Lead Contact, Je-Hyun Yoon (yoonje@musc.edu).

323

324 **Experimental Models and Subject Details**

325 *Cell culture, transfection, short hairpin RNAs, and plasmids*

326   Human HeLa, Mouse Embryonic Fibroblast (MEF), and HCT116 cells were cultured in DMEM

327 (Invitrogen) supplemented with 10% (v/v) FBS and antibiotics. Using PEI (polyethylenimine), the cells

328 were then transfected with shRNA plasmids designed to luciferase (5'-

329 CGCTGAGTACTTCGAAATGTC-3'), or QKI (5'-GCTCAGAACAGAGCAGAAATC-3'). pcDNA3.1

330 and pDESTmycQKI (Addgene, #19870) were used for overexpression experiments. Cells were analyzed

331 for RT-qPCR, western blot, and exosome purification 48 hours after transfection. To construct C-

332 terminal deletion mutant (CK-truncated) QKI, the corresponding DNA region was first amplified from

333 the pDESTmycQKI. The resulting PCR products were then sub-cloned the the *SalI* and *NotI* sites of the

334 pDESTmycQKI plasmid after removing full length QKI sequences. To construct luciferase reporter

335 vector containing the 3'UTR of *cMYC* mRNA, the full-length (FL) and minimum (Min) containing let-

336 7b binding site of 3' UTR of *cMYC* was cloned into the pmiRGLO Dual-Luciferase miRNA target

337 expression vector (Promega). *cMYC* 3' UTR region was first amplified from genomic DNA. Primer

338 sequences are listed in Table S6.

339

340 *RNP analysis*

341   For immunoprecipitation (IP) of RNP complexes from cell lysates [RIP analysis] (Yoon *et al*,

342   2012), cells were lysed in Protein Extraction Buffer (PEB) with 20 mM Tris-HCl at pH 7.5, 100 mM

343   KCl, 5 mM MgCl$_2$ and 0.5% NP-40 for 10 min on ice, and centrifuged at 10,000 × g for 15 min at 4°C.

344   The supernatant was then incubated 1 hour at 4°C with protein A-Sepharose beads coated with

345   antibodies recognizing QKI (ab126742), AGO2 (ab57113), Myc (sc-40), or control IgG (Santa Cruz

346   Biotechnology). After the beads were washed with NT2 buffer (50 mM Tris-HCl at pH 7.5, 150 mM

347   NaCl, 1 mM MgCl$_2$ and 0.05% NP-40), the complexes were incubated for 15 minutes at 37°C with 20

348   units of RNase-free DNase I. They were finally incubated for 15 minutes at 55 °C with 0.1% SDS and

349   0.5 mg/ml Proteinase K, to remove remaining DNA and proteins, respectively. The RNA isolated from

350   the IP materials was further assessed by Reverse transcription and quantitative PCR (RT-qPCR) analysis

351   using the primers (**Table S6**). Normalization of RIP results was carried out by quantifying, in parallel,

352   the relative levels of housekeeping RNAs such as *GAPDH* mRNA and *U6* snRNA in each IP sample.

353   These abundant RNAs are non-specifically recovered during IP reactions.

354

Western blot analysis

356   Whole-cell lysates prepared in PEB were separated by SDS-polyacrylamide gel electrophoresis

357   (SDS-PAGE) and transferred onto nitrocellulose membranes (Invitrogen iBlot Stack). Anti-β-Actin (sc-

358   47778) and anti-cMyc (sc-40) antibodies were purchased from Santa Cruz Biotechnology. Anti-Dicer

359   (ab82539), anti-AGO2 (ab57113) and anti-QKI (ab126742) antibodies were purchased from Abcam.

360   anti-GAPDH (2118S), endogenous c-Myc (D84C12) antibodies were purchased from Cell Signaling

361   Technology. Anti-pan AGO (MABE56) and anti-Flag antibody (SLBX2256) antibodies were purchased

362   from Sigma. The HRP-conjugated secondary antibodies were purchased from GE Healthcare.

363

364   *RNA analysis*

365   For RIP analysis, Ribozole (Amresco) was used to extract total RNA, and acidic phenol

366   (Ambion) was used to extract RNA. Reverse transcription (RT) was performed using random hexamers

367   and reverse transcriptase (Maxima, Thermo Scientific), and real-time, quantitative (q)PCR using gene-

368   specific primers (**Table S6**), and SYBR green master mix (Kapa Biosystems), using a BioRad iCycler

369   instrument.

370   MicroRNA quantitation was performed after RNA extraction from immunoprecipitated samples

371   (with anti-AGO2 antibody or control IgG), polyadenylation (QuantiMiR kit), and hybridization with

372   oligo-dT adaptors. After RT, cDNAs were quantitated by qPCR with microRNA-specific primers, or

373   with primers to detect the control transcript *U6* snRNA, along with a universal primer. *U6* snRNA was

374   used a normalization of exosomal miRNA (Xu *et al*, 2017; Zhang *et al*, 2018)

375

376   ***Single-molecule assay***

377   This assay was performed according to modifications of a previously described method (Jo *et al.*,

378   2015) (Yoon *et al.*, 2015). Quartz slides and coverslips were cleaned in piranha solution (3:1 solution of

379   concentrated sulfuric acid and 30% [v/v] hydrogen peroxide) for 20 min, and coated with 40:1 mixture

380   of polyethylene glycol (MPEG-SVA-5000; Laysan Bio) and biotinylated polyethylene glycol (Biotin-

381   PEG-SVA-5000; Laysan Bio). A detection chamber was assembled by sandwiching double-sided sticky

382   tape (3M) between a quartz slide and a coverslip. Polyethylene tubing (PE50; Becton Dickinson) was

383   connected to the inlet and outlet of the chamber for stable buffer exchange during fluorescence signal

384   measurement. For surface immobilization of target RNAs, streptavidin (0.2 mg/ml; Invitrogen) and

385   target RNA (50 pM) were sequentially injected into the flow-cell (detection chamber) and incubated for

386   2 min. To establish the AGO2:let-7b complex, let-7b miRNA (40 nM) was incubated with excess human

387   Argonaute 2 (1 μM; Sino Biological) at 23°C for 1 hour.

388   Fluorescence measurements were carried out with an oxygen-scavenging imaging buffer which

389   contained 20 mM Tris-HCl (pH 8.0), 135 mM KCl, 1mM $MgCl_2$, 1 mM Trolox (Sigma), 1 mg/mL

390   glucose oxidase (Sigma), 0.04 mg/ml catalase (Sigma), 0.4% (w/v) glucose (Sigma), and 2000 U/ml

391   RNase inhibitor (Promega). A single-molecule fluorescence image was taken using a home-built prism-

392   type Total Internal Reflection Fluorescence Microscope (TIRFM) equipped with an electron-multiplying

393   CCD camera (IXON DV597ECS-BV; Andor Technology) at a frame rate of 1 Hz (Roy *et al*, 2008) with

394   alternating laser excitation. The temperature of the flow-cell and solution was maintained at 37°C with a

395   temperature control system (Live Cell Instruments).

396

397   *High throughput RNA sequencing*

398   Total RNA was isolated from human HeLa cells transfected with control or QKI shRNA using

399   TRIzol according to manufacturer's instructions. For RNA-sequencing, we followed standard Illumina

400   sequencing protocols using the TruSeq Stranded Total RNA kit and NovaSeq6000 S4 (150bp PE). The

401   resulting data were aligned to human genome sequences (HG19) for assembly and quantitation.

402

403   *Small RNA sequencing and analysis*

404   Library preparation was performed using the TruSeq Small RNA library preparation kit

405   (Illumina, RS-200) following the manufacturer's instructions. Briefly, 1 μg of input RNA was loaded

406   into Urea-TBE gels for purification and the resulting RNAs were applied for the following procedures.

407   User-supplied reagents including T4 RNA ligase2 Deletion Mutant (Lucigen, LR2D1132K) and

408   Maxima First Stand cDNA synthesis kit (Thermo Fisher Scientific, K1641) were purchased separately.

409 Libraries were amplified using 11 cycles of PCR for the manufacture's index or modified index primer

410 set to increase diversity. Libraries were prepared according to the manufacturer's protocol with a

411 modification in the size selection step, which, instead of agarose gel purification, PippinHT Prep

412 instrument (Sage Science, HTP0001) and 3% agarose dye-free cassette with internal standards (Sage

413 Science, HTG3010) was used under the following conditions: base pair start = 120 bp, base pair end =

414 160 bp, range = broad, target peak size = 145 bp. Eluted Libraries from PippinHT system were

415 subsequently analyzed on Tape-station 4150 (Agilent Technologies, G2992AA) following the

416 manufacturer's instructions using a High Sensitivity DNA Screen tape (Agilent Technologies, 5067-

417 5584). Each library was barcoded with unique sequence of reverse primers during the PCR step, which

418 contained Illumina compatible indices and modified indexes (see GEO database). Before pooling

419 libraries for the next-generation sequencing, concentration of each library was measured in a high

420 sensitivity Tape-station followed by smear analysis. Illumina NextSeq 550 or Miniseq with single end

421 (50 nt;R1) read method was apply for the library sequencing.

422   Quality control and trimming of sequencing reads were performed using fastp (ref; fastp: an

423 ultra-fast all-in-one FASTQ preprocessor) with default parameter setting. Subsequently, reads shorter

424 than 15 bases were additionally excluded for the downstream analysis. The trimmed reads were mapped

425 based on mature and hairpin databases (Kozomara *et al*, 2019) for respective species (mouse or human)

426 after further clipped 3' Illumina stop oligo sequence (GAATTCCACCACGTTCCCGTGG). Then they

427 were quantified, and RPM (reads per million mapped reads) normalized. The mapping and

428 quantification steps were performed by mirDeep2 (Friedländer *et al*, 2012).

429

430 ***Chimera PCR***

431   This assay was slightly modified from previously described method (Broughton & Pasquinelli,

432   2018). In brief, cells were crosslinked using UV-C (254nm) crosslinker. After UV crosslinking, cells

433   were lysed with lysis buffer (20mM Tris-HCl pH 7.4, 10mM KCl, 5mM $MgCl_2$, 0.5% NP-40

434   supplemented with protease inhibitor cocktail, DTT, and RNase inhibitor), sonicated for 10 sec and

435   centrifuged at 17,000 x g for 15 min. Lysates were treated with RNase I (NEB) and Turbo DNase

436   (Invitrogen) to digest RNA not protected by Argonaute. Lysates were then immunoprecipitated using

437   anti-AGO2 antibody (Abcam) and Protein G dynabeads (Invitrogen). Beads were washed with high-salt

438   wash buffer (50mM Tris-HCl pH 7.4, 1M NaCl, 1mM EDTA, 1% NP-40, 0.1% SDS, 0.5% sodium

439   deoxycholate) and low-salt wash buffer (20mM Tris-HCl pH 7.4, 10mM $MgCl_2$, 0.2% Tween-20). The

440   5' end of target RNA was phosphorylated using T4 PNK 3' phosphatase minus (NEB) and 1mM ATP

441   (NEB) for 10 min at 37°C with shaking. The beads were then washed with low-salt wash buffer.

442   Intermolecular ligation of miRNA and target RNA was performed with T4 RNA ligase I (NEB), 1mM

443   ATP and PEG400 for overnight at 16°C. The beads were then washed with low-salt wash buffer. The 3'

444   phosphate left over after RNase I digestion was removed using T4 PNK (NEB) and the ligation of the 3'

445   linker was performed using T4 RNA ligase I (NEB). After linker ligation, the RNA was isolated using

446   proteinase K and reverse transcribed. cDNAs were then size selected to remove extra reverse

447   transcription primer using AMPure XP beads (Beckman Coulter). The cDNAs were circularized using

448   CirLligase II (Lucigen), linearized using BamHI (NEB) and libraries were then amplified using Taq

449   DNA polymerase (Enzynomics). Libraries containing residual primers were purified by AMPure XP

450   beads before specific-chimera amplification. Let-7b-*POLR2D* chimeras were detected by PCR

451   amplification using a forward primer matching the mature let-7b sequence and a reverse primer

452   complementary to the *POLR2D* target site and were detected by DNA polyacrylamide gel

453   electrophoresis. Primer sequences are listed in Table S6.

454

miRNA activity reporter assay

456   HeLa cells were seeded at a density of ~60% in a 12-well culture plate and incubated at 37°C.

457   After 24 hours of transfection, the cells were washed twice with PBS. Dual luciferase assay was

458   performed using the Dual luciferase reporter assay system (Promega, #E1910) according to

459   manufacturer's instructions.

460

Migration assay

462   Cell migration assays were performed using Transwell plates with 8.0 μm pore size membranes

463   (Falcon, #353097). The cells were seeded at 2.5 x 10^5 in 200 μl of serum-free medium and added to the

464   upper chamber of a 24-well plate. The lower chamber was filled with 750 μl of medium with serum. The

465   24-well plate was incubated at 37°C for 24 hours. Migrated cells on the bottom side of the membranes

466   were fixed with 4% formaldehyde in PBS for 15 minutes and the chamber was then washed with PBS.

467   The cells were permeabilized with PBS containing 0.25% X-100 for 10 minutes and the chamber was

468   washed again with PBS. Cells on the lower chamber membrane were stained with 0.5% crystal violet

469   dissolved in 20% methanol for 15 minutes and then the chamber was washed with PBS. Non-migrating

470   cells were scraped off with cotton swabs. Migrated cells were quantified using ImageJ.

471

Cell Proliferation assay

473   The cell proliferation was measured using the EZ-CYTOX (DoGen, #EZ-3000,) according to

474   manufacturer's instructions. Briefly, cells were seeded at 4 x 10^3 cells/well in 100 μl of culture medium

475   on a 96-well plate. After 24 hours, the cells were washed with PBS. The culture medium and EZ-

476   CYTOX reagent were then diluted at a ratio of 9:1 and 100 μl of the mixture was added to each well.

477   The 96-well plate was incubated at 37°C for 30 minutes. The absorbance at 450 nm was then measured

478   using a plate reader.

479

484

485 **DECLARATION OF INTERESTS**

486 The authors declare no competing interests.

REFERENCES

Abe M, Bonini NM (2013) MicroRNAs and neurodegeneration: role and impact. *Trends Cell Biol* 23: 30-36

Alles J, Fehlmann T, Fischer U, Backes C, Galata V, Minet M, Hart M, Abu-Halima M, Grässer FA, Lenhof H-P (2019) An estimate of the total number of true human miRNAs. *Nucleic Acids Res* 47: 3353-3364

Arluison V, Buckle M, Grosjean H (1999) Pseudouridine synthetase Pus1 of Saccharomyces cerevisiae: kinetic characterisation, tRNA structural requirement and real-time analysis of its complex with tRNA. *J Mol Biol* 289: 491-502

Baccarini A, Chauhan H, Gardner TJ, Jayaprakash AD, Sachidanandam R, Brown BD (2011) Kinetic analysis reveals the fate of a microRNA following target regulation in mammalian cells. *Curr Biol* 21: 369-376

Becker WR, Ober-Reynolds B, Jouravleva K, Jolly SM, Zamore PD, Greenleaf WJ (2019) High-throughput analysis reveals rules for target RNA binding and cleavage by AGO2. *Mol Cell* 75: 741-755. e711

Broughton JP, Lovci MT, Huang JL, Yeo GW, Pasquinelli AE (2016) Pairing beyond the Seed Supports MicroRNA Targeting Specificity. *Mol Cell* 64: 320-333

Broughton JP, Pasquinelli AE (2018) Detection of microRNA-Target Interactions by Chimera PCR (ChimP). *Methods Mol Biol* 1823: 153-165

Büssing I, Slack FJ, Großhans H (2008) let-7 microRNAs in development, stem cells and cancer. *Trends Mol Med* 14: 400-409

Chatterjee S, Großhans H (2009) Active turnover modulates mature microRNA activity in Caenorhabditis elegans. *Nature* 461: 546-549

Chen C, Ridzon DA, Broomer AJ, Zhou Z, Lee DH, Nguyen JT, Barbisin M, Xu NL, Mahuvakar VR, Andersen MR (2005) Real-time quantification of microRNAs by stem–loop RT–PCR. *Nucleic Acids Res* 33: e179-e179

Chen Y, Song Y, Huang J, Qu M, Zhang Y, Geng J, Zhang Z, Liu J, Yang G-Y (2017) Increased circulating exosomal miRNA-223 is associated with acute ischemic stroke. *Frontiers in neurology* 8: 57

Chiang HR, Schoenfeld LW, Ruby JG, Auyeung VC, Spies N, Baek D, Johnston WK, Russ C, Luo S, Babiarz JE (2010) Mammalian microRNAs: experimental evaluation of novel and previously annotated genes. *Genes Dev* 24: 992-1009

Ciafrè SA, Galardi S (2013) microRNAs and RNA-binding proteins: a complex network of interactions and reciprocal regulations in cancer. *RNA Biol* 10: 934-942

Conn SJ, Pillman KA, Toubia J, Conn VM, Salmanidis M, Phillips CA, Roslan S, Schreiber AW, Gregory PA, Goodall GJ (2015) The RNA binding protein quaking regulates formation of circRNAs. *Cell* 160: 1125-1134

Dang CV (2012) MYC on the path to cancer. *Cell* 149: 22-35

De Bruin RG, Shiue L, Prins J, De Boer HC, Singh A, Fagg WS, Van Gils JM, Duijs JM, Katzman S, Kraaijeveld AO (2016) Quaking promotes monocyte differentiation into pro-atherogenic macrophages by controlling pre-mRNA splicing and gene expression. *Nature communications* 7: 1-20

Diederichs S, Jung S, Rothenberg SM, Smolen GA, Mlody BG, Haber DA (2008) Coexpression of Argonaute-2 enhances RNA interference toward perfect match binding sites. *Proceedings of the National Academy of Sciences* 105: 9284-9289

Ding SL, Zhou LY, Li PF (2011) MicroRNAs in cardiac hypertrophy: angels or devils. *Wiley Interdisciplinary Reviews: RNA* 2: 124-134

Eiring AM, Harb JG, Neviani P, Garton C, Oaks JJ, Spizzo R, Liu S, Schwind S, Santhanam R, Hickey CJ (2010) miR-328 functions as an RNA decoy to modulate hnRNP E2 regulation of mRNA translation in leukemic blasts. *Cell* 140: 652-665

Elbarbary RA, Miyoshi K, Myers JR, Du P, Ashton JM, Tian B, Maquat LE (2017) Tudor-SN–mediated endonucleolytic decay of human cell microRNAs promotes G1/S phase transition. *Science* 356: 859-862

Fabian MR, Sonenberg N (2012) The mechanics of miRNA-mediated gene silencing: a look under the hood of miRISC. *Nat Struct Mol Biol* 19: 586-593

Friedländer MR, Mackowiak SD, Li N, Chen W, Rajewsky N (2012) miRDeep2 accurately identifies known and hundreds of novel microRNA genes in seven animal clades. *Nucleic Acids Res* 40: 37-52

Gehring NH, Wahle E, Fischer U (2017) Deciphering the mRNP code: RNA-bound determinants of post-transcriptional gene regulation. *Trends in biochemical sciences* 42: 369-382

Ghini F, Rubolino C, Climent M, Simeone I, Marzi MJ, Nicassio F (2018) Endogenous transcripts control miRNA levels and activity in mammalian cells by target-directed miRNA degradation. *Nature communications* 9: 1-15

Gleitsman KR, Sengupta RN, Herschlag D (2017) Slow molecular recognition by RNA. *RNA* 23: 1745-1753

Golden RJ, Chen B, Li T, Braun J, Manjunath H, Chen X, Wu J, Schmid V, Chang T-C, Kopp F (2017) An Argonaute phosphorylation cycle promotes microRNA-mediated silencing. *Nature* 542: 197-202

Gregory RI, Yan K-p, Amuthan G, Chendrimada T, Doratotaj B, Cooch N, Shiekhattar R (2004) The Microprocessor complex mediates the genesis of microRNAs. *Nature* 432: 235-240

553 Ha M, Kim VN (2014) Regulation of microRNA biogenesis. *Nature reviews Molecular cell biology* 15:
554 509-524

555 Hafner M, Landthaler M, Burger L, Khorshid M, Hausser J, Berninger P, Rothballer A, Ascano Jr M,
556 Jungkamp A-C, Munschauer M (2010) Transcriptome-wide identification of RNA-binding protein and
557 microRNA target sites by PAR-CLIP. *Cell* 141: 129-141

558 Han J, LaVigne CA, Jones BT, Zhang H, Gillett F, Mendell JT (2020) A ubiquitin ligase mediates target-
559 directed microRNA decay independently of tailing and trimming. *Science* 370: eabc9546

560 Jackson RJ, Hellen CU, Pestova TV (2010) The mechanism of eukaryotic translation initiation and
561 principles of its regulation. *Nature reviews Molecular cell biology* 11: 113-127

562 Jo MH, Shin S, Jung S-R, Kim E, Song J-J, Hohng S (2015) Human Argonaute 2 has diverse reaction
563 pathways on target RNAs. *Molecular cell* 59: 117-124

564 Jonas S, Izaurralde E (2015) Towards a molecular understanding of microRNA-mediated gene
565 silencing. *Nature reviews genetics* 16: 421-433

566 Katoh T, Sakaguchi Y, Miyauchi K, Suzuki T, Kashiwabara S-i, Baba T, Suzuki T (2009) Selective
567 stabilization of mammalian microRNAs by 3′ adenylation mediated by the cytoplasmic poly (A)
568 polymerase GLD-2. *Genes Dev* 23: 433-438

569 Kawamata T, Seitz H, Tomari Y (2009) Structural determinants of miRNAs for RISC loading and slicer-
570 independent unwinding. *Nat Struct Mol Biol* 16: 953-960

571 Kim Y-K, Kim B, Kim VN (2016) Re-evaluation of the roles of DROSHA, Exportin 5, and DICER in
572 microRNA biogenesis. *Proceedings of the National Academy of Sciences* 113: E1881-E1889

573 Kingston ER, Bartel DP (2019) Global analyses of the dynamics of mammalian microRNA metabolism.
574 *Genome Res* 29: 1777-1790

575 Kingston ER, Bartel DP (2021) Ago2 protects Drosophila siRNAs and microRNAs from target-directed
576 degradation, even in the absence of 2′-O-methylation. *RNA* 27: 710-724

577 Kleaveland B, Shi CY, Stefano J, Bartel DP (2018) A network of noncoding regulatory RNAs acts in the
578 mammalian brain. *Cell* 174: 350-362. e317

579 Kozomara A, Birgaoanu M, Griffiths-Jones S (2019) miRBase: from microRNA sequences to function.
580 *Nucleic Acids Res* 47: D155-D162

581 Larocque D, Pilotte J, Chen T, Cloutier F, Massie B, Pedraza L, Couture R, Lasko P, Almazan G,
582 Richard S (2002) Nuclear retention of MBP mRNAs in the quaking viable mice. *Neuron* 36: 815-829

583 Lee D, Park D, Park JH, Kim JH, Shin C (2019) Poly (A)-specific ribonuclease sculpts the 3′ ends of
584 microRNAs. *RNA* 25: 388-405

585 Lee Y, Ahn C, Han J, Choi H, Kim J, Yim J, Lee J, Provost P, Rådmark O, Kim S (2003) The nuclear
586 RNase III Drosha initiates microRNA processing. *Nature* 425: 415-419
587 Li J, Yang Z, Yu B, Liu J, Chen X (2005) Methylation protects miRNAs and siRNAs from a 3′-end
588 uridylation activity in Arabidopsis. *Curr Biol* 15: 1501-1507
589 Martinez NJ, Gregory RI (2013) Argonaute2 expression is post-transcriptionally coupled to microRNA
590 abundance. *Rna* 19: 605-612
591 Marzi MJ, Ghini F, Cerruti B, De Pretis S, Bonetti P, Giacomelli C, Gorski MM, Kress T, Pelizzola M,
592 Muller H (2016) Degradation dynamics of microRNAs revealed by a novel pulse-chase approach.
593 *Genome Res* 26: 554-565
594 Massey VL, Qin L, Cabezas J, Caballeria J, Sancho-Bru P, Bataller R, Crews FT (2018) TLR 7-let-7
595 Signaling Contributes to Ethanol-Induced Hepatic Inflammatory Response in Mice and in Alcoholic
596 Hepatitis. *Alcoholism: Clinical and Experimental Research* 42: 2107-2122
597 Meškytė EM, Keskas S, Ciribilli Y (2020) MYC as a Multifaceted Regulator of Tumor Microenvironment
598 Leading to Metastasis. *International Journal of Molecular Sciences* 21: 7710
599 Min K-W, Jo MH, Shin S, Davila S, Zealy RW, Kang SI, Lloyd LT, Hohng S, Yoon J-H (2017) AUF1
600 facilitates microRNA-mediated gene silencing. *Nucleic Acids Res* 45: 6064-6073
601 Min KW, Evans JG, Won EC, Yoon JH (2020) Detection of MicroRNAs Released from Argonautes.
602 *Methods Mol Biol* 2106: 151-159
603 Misiewicz-Krzeminska I, Krzeminski P, Corchete LA, Quwaider D, Rojas EA, Herrero AB, Gutiérrez NC
604 (2019) Factors regulating microRNA expression and function in multiple myeloma. *Non-coding RNA* 5:
605 9
606 O'Carroll D, Mecklenbrauker I, Das PP, Santana A, Koenig U, Enright AJ, Miska EA, Tarakhovsky A
607 (2007) A Slicer-independent role for Argonaute 2 in hematopoiesis and the microRNA pathway. *Genes*
608 *Dev* 21: 1999-2004
609 Park-Lee S, Kim S, Laird-Offringa IA (2003) Characterization of the interaction between neuronal RNA-
610 binding protein HuD and AU-rich RNA. *Journal of Biological Chemistry* 278: 39801-39808
611 Park S, Myszka DG, Yu M, Littler SJ, Laird-Offringa IA (2000) HuD RNA recognition motifs play distinct
612 roles in the formation of a stable complex with AU-rich RNA. *Molecular and cellular biology* 20: 4765-
613 4772
614 Reichholf B, Herzog VA, Fasching N, Manzenreither RA, Sowemimo I, Ameres SL (2019) Time-
615 resolved small RNA sequencing unravels the molecular principles of microRNA homeostasis. *Mol Cell*
616 75: 756-768. e757
617 Roy R, Hohng S, Ha T (2008) A practical guide to single-molecule FRET. *Nat Methods* 5: 507-516

618 Ruby JG, Jan CH, Bartel DP (2007) Intronic microRNA precursors that bypass Drosha processing.
619 *Nature* 448: 83-86

620 Rupaimoole R, Calin GA, Lopez-Berestein G, Sood AK (2016) miRNA deregulation in cancer cells and
621 the tumor microenvironment. *Cancer Discov* 6: 235-246

622 Salomon WE, Jolly SM, Moore MJ, Zamore PD, Serebrov V (2015) Single-molecule imaging reveals
623 that argonaute reshapes the binding properties of its nucleic acid guides. *Cell* 162: 84-95

624 Sheedy FJ (2015) Turning 21: induction of miR-21 as a key switch in the inflammatory response.
625 *Frontiers in immunology* 6: 19

626 Shen K, Shan S-o (2010) Transient tether between the SRP RNA and SRP receptor ensures efficient
627 cargo delivery during cotranslational protein targeting. *Proceedings of the National Academy of*
628 *Sciences* 107: 7698-7703

629 Sheu-Gruttadauria J, Pawlica P, Klum SM, Wang S, Yario TA, Oakdale NTS, Steitz JA, MacRae IJ
630 (2019) Structural basis for target-directed microRNA degradation. *Mol Cell* 75: 1243-1255. e1247

631 Shi CY, Kingston ER, Kleaveland B, Lin DH, Stubna MW, Bartel DP (2020) The ZSWIM8 ubiquitin
632 ligase mediates target-directed microRNA degradation. *Science* 370: eabc9359

633 Shukla S, Bjerke GA, Muhlrad D, Yi R, Parker R (2019) The RNase PARN controls the levels of specific
634 miRNAs that contribute to p53 regulation. *Molecular cell* 73: 1204-1216. e1204

635 Thangaraj MP, Furber KL, Gan JK, Ji S, Sobchishin L, Doucette JR, Nazarali AJ (2017) RNA-binding
636 protein quaking stabilizes Sirt2 mRNA during oligodendroglial differentiation. *J Biol Chem* 292: 5166-
637 5182

638 Towler BP, Jones CI, Newbury SF (2015) Mechanisms of regulation of mature miRNAs. *Biochem Soc*
639 *Trans* 43: 1208-1214

640 Wang Y, Lacroix G, Haines J, Doukhanine E, Almazan G, Richard S (2010a) The QKI-6 RNA binding
641 protein localizes with the MBP mRNAs in stress granules of glial cells. *PLoS One* 5: e12824

642 Wang Z, Li Y, Ahmad A, Azmi AS, Kong D, Banerjee S, Sarkar FH (2010b) Targeting miRNAs involved
643 in cancer stem cell and EMT regulation: An emerging concept in overcoming drug resistance. *Drug*
644 *resistance updates* 13: 109-118

645 Wu JI, Reed RB, Grabowski PJ, Artzt K (2002) Function of quaking in myelination: regulation of
646 alternative splicing. *Proceedings of the National Academy of Sciences* 99: 4233-4238

647 Xu J-F, Wang Y-P, Zhang S-J, Chen Y, Gu H-F, Dou X-F, Xia B, Bi Q, Fan S-W (2017) Exosomes
648 containing differential expression of microRNA and mRNA in osteosarcoma that can predict response
649 to chemotherapy. *Oncotarget* 8: 75968

Yamamichi N, Shimomura R, Inada K-i, Sakurai K, Haraguchi T, Ozaki Y, Fujita S, Mizutani T, Furukawa C, Fujishiro M (2009) Locked nucleic acid in situ hybridization analysis of miR-21 expression during colorectal cancer development. *Clinical cancer research* 15: 4009-4016

Yang J-S, Maurin T, Robine N, Rasmussen KD, Jeffrey KL, Chandwani R, Papapetrou EP, Sadelain M, O'Carroll D, Lai EC (2010) Conserved vertebrate mir-451 provides a platform for Dicer-independent, Ago2-mediated microRNA biogenesis. *Proceedings of the National Academy of Sciences* 107: 15163-15168

Yoon J-H, Abdelmohsen K, Gorospe M (2013a) Posttranscriptional gene regulation by long noncoding RNA. *J Mol Biol* 425: 3723-3730

Yoon J-H, Abdelmohsen K, Kim J, Yang X, Martindale JL, Tominaga-Yamanaka K, White EJ, Orjalo AV, Rinn JL, Kreft SG (2013b) Scaffold function of long non-coding RNA HOTAIR in protein ubiquitination. *Nature communications* 4: 1-14

Yoon J-H, Abdelmohsen K, Srikantan S, Yang X, Martindale JL, De S, Huarte M, Zhan M, Becker KG, Gorospe M (2012) LincRNA-p21 suppresses target mRNA translation. *Mol Cell* 47: 648-655

Yoon J-H, Jo MH, White EJ, De S, Hafner M, Zucconi BE, Abdelmohsen K, Martindale JL, Yang X, Wood WH (2015) AUF1 promotes let-7b loading on Argonaute 2. *Genes Dev* 29: 1599-1604

Zangari J, Ilie M, Rouaud F, Signetti L, Ohanna M, Didier R, Roméo B, Goldoni D, Nottet N, Staedel C (2017) Rapid decay of engulfed extracellular miRNA by XRN1 exonuclease promotes transient epithelial-mesenchymal transition. *Nucleic Acids Res* 45: 4131-4141

Zealy RW, Wrenn SP, Davila S, Min KW, Yoon JH (2017) microRNA-binding proteins: specificity and function. *Wiley Interdisciplinary Reviews: RNA* 8: e1414

Zhang M, Zhou Z, Wang J, Li S (2016) MiR-130b promotes obesity associated adipose tissue inflammation and insulin resistance in diabetes mice through alleviating M2 macrophage polarization via repression of PPAR-γ. *Immunology Letters* 180: 1-8

Zhang W, Ni M, Su Y, Wang H, Zhu S, Zhao A, Li G (2018) MicroRNAs in serum exosomes as potential biomarkers in clear-cell renal cell carcinoma. *European urology focus* 4: 412-419

Zhu Y, Xu G, Yang YT, Xu Z, Chen X, Shi B, Xie D, Lu ZJ, Wang P (2019) POSTAR2: deciphering the post-transcriptional regulatory logics. *Nucleic Acids Res* 47: D203-D211

679   **FIGURE LEGEND**

680

681   **Figure 1. PAR-CLIP analysis identified RNA-binding proteins directly binding with mature and**

682   **precursor miRNAs.**

683   **(A - C)** Genome coordinates (y-axis) of precursor and mature miRNA let-7a-1 (A), 7b (B), and 7c (C)

684   identified from PAR-CLIP using human cell lines. T-to-C conversion ratio was presented in y-axis as

685   well. Representative RBPs such as QKI, HuR, hnRNPD/AUF1 and IGF2BP were highlighted.

686
687

688   **Figure 2. Existence of AGO-free mature miRNAs in human and mouse cells.**

689   **(A)** Schematic of experimental set up to profile mature miRNAs from AGO-depleted human and mouse

690   cell lysates. HeLa or MEF lysates were immunoprecipitated using anti-AGO2 or anti-Pan AGO

691   antibodies serially. The resulting pellets and lysates were subjected to RNA purification followed by

692   high throughput RNA-sequencing or RT-qPCR.

693   **(B)** Western blot analysis of AGO2, QKI and ACTB using cell lysates before and after serial

694   immunoprecipitation.

695   **(C, D)** RNA-seq analysis of let-7, miR-21 and miR-130b using cell lysates before and after

696   immunoprecipitation with anti-AGO2 or anti-Pan AGO antibodies. N = 2-4, n.d., not detected from

697   RNA-seq, ***$p < 0.001$, **$p < 0.01$, *$p < 0.05$, *n.s.*, not significant from Student's *t*-test. Data are mean

698   ± S.D.

699   **(E)** Western blot analysis of AGO2, Pan-AGO, DICER, QKI and ACTB using cell lysates HCT116 cells

700   targeting AGO1, 2, and 3. RNA-seq analysis of let-7, miR-21, miR-130b, and miR-100 using HCT116

701   wild type and AGO TKO cells. N = 2, ***$p < 0.001$, *$p < 0.05$, *n.s.*, not significant from Student's *t*-

702   test. Data are mean ± S.D.

703 **(F)** Scatter plots of miRNAs sequenced from HCT116 wild type and AGO TKO cells.

704 **(G)** Counting of let-7b from 2 ng total RNA purified from HCT116 wild type and AGO TKO cells. N =

705 6, *n.s.*, not significant from Student's *t*-test. Data are mean ± S.D.

706

707 **Figure 3. QKI is required for AGO2 interaction with let-7b and allows let-7b loading onto AGO2.**

708 **(A)** A model of QKI's effect on interaction of AGO2 and let-7b in human cells.

709 **(B)** AGO2 RIP assay in HeLa cells after transfection of control and QKI shRNA. (*Left*) At 48 hours

710 after transfection of shRNA targeting GFP or QKI in HeLa cells, cell lysates were subjected to

711 immunoprecipitation against AGO2 for detection of co-purified let-7b by RT-qPCR. (*Middle*) At 48

712 hours after transfection of shRNA targeting GFP or QKI in HeLa cells, total RNAs were purified for

713 detection of let-7b by RT-qPCR. (*Right*) Efficiency of QKI shRNA was determined by western blot of

714 total cell lysates with anti-QKI or anti-ACTB antibodies. N = 3, **$p < 0.01$, *n.s.*, not significant from

715 Student's *t*-test. Data are mean ± S.D. Data are mean ± S.D.

716 **(C)** A model of QKI's effect on let-7b loading on AGO2 in single molecule analysis.

717 **(D)** Single-molecule experimental scheme for let-7b (guide RNA) loading on AGO2. Recombinant

718 AGO2 was immobilized on PEG-passivated surface using avidin-biotin interaction and anti-His tag

719 antibody in a detection chamber. Cy5-labeled let-7b was injected into the chamber with or without QKI

720 during the imaging.

721 **(E)** Histograms of let-7b loading times in (*Left*) absence or (*Right*) presence of recombinant OKI. The

722 red lines are single exponential decay fit (27 s and 130 s, respectively).

723 **(F)** Single exponential fit was performed for loading time distributions. Loading rates of let-7b onto

724 immobilized AGO2 with or without QKI. About 300-500 loading events were observed per

725 experiment. N = 3, **$p < 0.01$, from Student's *t*-test. Data are mean ± S.D.

726   **(G)** Cy5-labeled let-7b spots on slides with or without immobilized AGO2 and QKI 5 minutes after let-

727   7b injection. The results of single-molecule assay.

728   **(H)** Recombinant QKI and AGO2 were visualized by Coomassie Blue staining and let-7b is imaged by

729   ethidium bromide staining. The abundance of let-7b was assessed by reverse transcriptase PCR

730   analysis.

731

732   **Figure 4. QKI is essential for let-7b-mediated mRNA decay.**

733   **(A)** AGO2 RIP assay was performed in HeLa cells after transfection of control and QKI shRNA for

734   detection of *POLR2D* mRNA. (*Left*) After AGO2 RIP, the amount of *POLR2D* mRNA (a let-7b target

735   mRNA) from immune pellets were determined by reverse transcription (RT) and qPCR, with

736   normalization to *TUBA* mRNA. (*Right*) Total RNAs were extracted from control and QKI shRNA cells

737   for RT- qPCR. N = 3, **$p < 0.01$, *$p < 0.05$, not significant from Student's *t*-test. Data are mean ± S.D.

738   **(B)** AGO2 RIP samples were subjected to SDS-PAGE for western blot analysis against AGO2, QKI

739   and ACTB.

740   **(C)** Measurement of *POLR2D* and *GAPDH* mRNA stability with Actinomycin D treatment after

741   transfection of control or QKI shRNA in HeLa cells. At a given time of Actinomycin D treatment, total

742   RNA was purified and converted into cDNA for quantitation of *POLR2D*, *GAPDH* mRNA, or *18S*

743   RNA. The stability of (*Left*) *POLR2D* and (*Right*) *GAPDH* mRNAs were determined by comparing the

744   remaining amounts of mRNA to the pre-treatment levels, which were normalized using 18S RNA. N =

745   3, *$p < 0.05$, *n.s.*, not significant from Student's *t*-test. Data are mean ± S.D.

746   **(D)** Measurement of *LUC2* reporter and *GAPDH* mRNA stability after transfection of control and QKI

747   shRNA in HeLa cells. After treatment of Actinomycin D, stability of *LUC2 (Left)* and *GAPDH*

748   mRNAs (*Right*) were assessed by RT-qPCR with normalization of *18S* RNA (WT QKI shRNA vs WT

749 control/mutant control/mutant QKI). N = 3, *$p < 0.05$, *n.s.*, not significant from Student's *t*-test. Data

750 are mean ± S.D.

751 **(E)** AGO2 RIP assay using lysates from HeLa cells after transfection of empty vector and Myc- QKI

752 overexpression plasmids for detection of *POLR2D* mRNA. (*Left*) After AGO2 RIP, the amount of

753 *POLR2D* mRNA from immune pellets were determined by RT-qPCR with normalization to *TUBA*

754 mRNA. (*Right*) Steady-state level of *POLR2D* mRNA was measured by RT-qPCR using total RNAs

755 extracted from control and QKI shRNA. N = 3, **$p < 0.01$, *$p < 0.05$, from Student's *t*-test. Data are

756 mean ± S.D.

757 **(F)** AGO2 IP efficiency was verified after AGO2 immunoprecipitation and western blot analysis using

758 lysates from HeLa cells transfected with control or Myc-QKI plasmids.

759

760 **Figure 5. C-terminal region of QKI is essential for AGO2-mediated mRNA decay.**

761 **(A)** (*Left*) AGO2 RIP samples were subjected to SDS-PAGE for western blot analysis against QKI, c-

762 Myc and GAPDH. (*Middle*) MYC RIP and (*Right*) AGO2 RIP and let-7b RT-qPCR assay were

763 performed in HeLa cells transfected with control shRNA or QKI shRNA in combination with QKI full

764 length or CK mutant plasmids. At 48 hours after transfection, cell lysates were subjected to

765 immunoprecipitation against AGO2 for enrichment of co-purified let-7b by RT-qPCR. N = 2, ***$p <$

766 0.001, *$p < 0.05$, *n.s.*, not significant from Student's *t*-test. Data are mean ± S.D.

767 **(B)** RT-qPCR levels of let-7b using RNAs purified from the corresponding samples. N = 2, *n.s.*, not

768 significant from Student's *t*-test. Data are mean ± S.D.

769 **(C)** Measurement of *POLR2D* mRNA (*Left*) and *GAPDH* mRNA stability (*Right*) after re-introducing

770 QKI full length or CK mutant in QKI knockdown cells. After treatment of Actinomycin D, stability of

771 *POLR2D* and *GAPDH* mRNAs were assessed by RT-qPCR with normalization of *18S* RNA. N = 2, *p

772   < 0.05, *n.s.* not significant from Student's *t*-test. Data are mean ± S.D.

773   **(D)** Measurement of *POLD2D* mRNA (*Left*) and *GAPDH* mRNA (*Right*) stability after transfection of

774   Flag-tagged AGO2 expression or empty vector in HeLa cells either stably expressing control shRNA or

775   QKI shRNA. After treatment of Actinomycin D, stability of *POLR2D* and *GAPDH* mRNAs were

776   assessed by RT-qPCR with normalization of *18S* RNA. N = 2, *$*p$ < 0.05, *n.s.*, not significant from

777   Student's *t*-test. Data are mean ± S.D.

778   **(E)** *POLR2D* mRNA stability assay samples were subjected to SDS-PAGE for western blot analysis

779   against Flag, QKI and GAPDH antibodies.

780

781   **Figure 6. QKI slows down AGO2-let-7b-target RNA assembly and suppresses let-7b release.**

782   **(A)** Detection of let-7b released from recombinant AGO2 *in vitro*. AGO2 in complex with let-7b was

783   immobilized on the sepharose beads for detection of let-7b from the supernatant, in the presence of

784   GST or QKI using RT-qPCR. N = 3, *$*p$ < 0.05, from Student's *t*-test. Data are mean ± S.D.

785   **(B)** Detection of let-7b and *POLR2D* mRNA released from AGO2 *in vivo*. AGO2 in complex with let-7b

786   and *POLR2D* mRNA was immobilized on the sepharose beads using HeLa cell lysates for detection of

787   let-7b from the supernatant, in the presence of GST or QKI using RT-qPCR. N = 3, **$**p$ < 0.01, from

788   Student's *t*-test. Data are mean ± S.D.

789   **(C)** Target RNA sequence of *POLR2D* 3' UTR fragment containing let-7b site. Cy3 was labeled at the

790   5'-end and biotin was labeled at the 3'-end.

791   **(D)** Single-molecule assay of RISC assembly with target RNA in the presence of QKI. The RISC

792   solution (AGO2 and let-7b) was injected into the chamber in the presence or absence of excessive QKI

793   (100 nM) with pre-incubation for 5 minutes.

794   **(E)** Representative time trace of fluorescence of Cy3 on *POLR2D* fragment. The RISC solution was

795   injected into the chamber at 40 s (dashed line).

796   **(F)** The binding rate of let-7b to *POLR2D* target was obtained through single exponential fit of the

797   binding time histogram. The number of data is > 330 each. N = 3, *$p < 0.05$, *n.s.*, not significant from

798   Student's *t*-test. Data are mean ± S.D.

799   **(G, H)** Histograms of binding time in (G) absence or (H) presence of recombinant OKI. The red lines

800   are single exponential decay fit (17 s and 70 s, respectively), N = 3.

Figure S1. PAR-CLIP analysis identified RNA-biding proteins directly binding with mature and precursor let-7.

(A, B) Genome coordinates (y-axis) of precursor and mature miRNA let-7a-2 (A, *Left*), 7a-3 (A, *Right*), and 7d (B) identified from PAR-CLIP using human cell lines. T-to-C conversion ratio was presented in y-axis as well. Representative RBPs such as QKI and HuR were highlighted.

**(C)** Venn diagram of common RBPs directly binding with let-7a, 7b, 7c, and 7d.

(D) We analyzed human QKI PAR-CLIP by sorting miRNAs in the order of T-to-C conversion counts: the top 20 miRNAs are listed.

Figure S2. PAR-CLIP analysis identified RNA-biding proteins directly binding with mature and precursor miR-21 and miR-130b.

(A, B) Genome coordinates (y-axis) of precursor and mature miRNA miR-21 (*Top*) and miR-130b (*Bottom*) identified from PAR-CLIP using human cell lines. T-to-C conversion ratio was presented in y-axis as well. Representative RBPs such as QKI, HuR and hnRNPD/AUF1 were highlighted.

(C) Venn diagram of common RBPs directly binding with let-7b, miR-21, and miR-130b.

Figure S3. Assay of mature miRNAs when AGOs are depleted.

(A) Level of let-7b was measured by miRNA counting (*Left*) and mature miRNA let-7, miR-130b and miR-21 levels were measured by RNA-seq (*Right*) using RNAs purified from wild type, AGO1 (Talen) KO, AGO2 (Talen) KO, or AGO1/2 DKO (Talen/CRISPR) HeLa cells. N = 2, *$p < 0.05$, *n.s.*, not significant from Student's *t*-test. Data are mean ± S.D.

(B) Scatter plots of passenger strand miRNAs from RNA-seq of HCT116 wild type and AGO TKO cells.

(C) Levels of let-7 miRNAs were measured by RNA-seq (*Left*) and by miRNA counting (*Right*) using

824   wild type, Dicer1 KO or Ago2 KO MEFs. (*Bottom*) Western blot analysis of Dicer1 and ACTB using

825   MEF lysates. n.d., not detected from RNA-seq, **$p < 0.01$, *$p < 0.05$, *n.s.*, not significant from

826   Student's *t*-test. Data are mean ± S.D.

827   **(D)** Stability of let-7b (*Left*), miR-21 (*Middle*), and miR-130b (*Right*) calculated from RT-qPCR using

828   RNAs purified from wild type, Ago2 KO or Dicer1 KO MEFs treated with Actinomycin D at a given

829   time point.

830

831   **Figure S4. QKI suppresses proliferation and migration of cancer cell by enhancing 1et-7b**

832   **activity.**

833   **(A)** Luciferase reporter analysis for let-7b activity after transfected with QKI overexpression plasmid

834   in HeLa cells. N = 3, ****p < 0.001*, **p < 0.05* from Student's *t*-test. Data are mean ± S.D.

835   **(B)** Western blot analyses of endogenous cMYC protein expression in HeLa cells transfected with

836   either control or QKI overexpression plasmids.

837   **(C)** Proliferation assay of HeLa cells that transfected with QKI overexpression plasmid. N = 4, ****p <*

838   *0.001* from Student's *t*-test. Data are mean ± S.D.

839   **(D)** Migration assay in HeLa cells after QKI overexpression. N = 3, ****p < 0.001* from Student's *t*-test.

840   Data are mean ± S.D.

841

842   **Figure S5. QKI stabilizes let-7b-*POLR2D* mRNA interaction.**

843   **(A)** Schematic representation of the main steps of Chimera PCR.

844   **(B)** Detection of let-7b binding to the 3' UTR of *POLR2D* mRNA using Chimera PCR after

845   transfection of either control or QKI shRNAs in HeLa cells.

846   **(C)** Cumulative-distribution fraction plots (CDF) depicting the let-7b target RNAs fold change upon

847   QKI knockdown. Significance was determined using a two-sided Kolmogorov–Smirnov (KS) test.
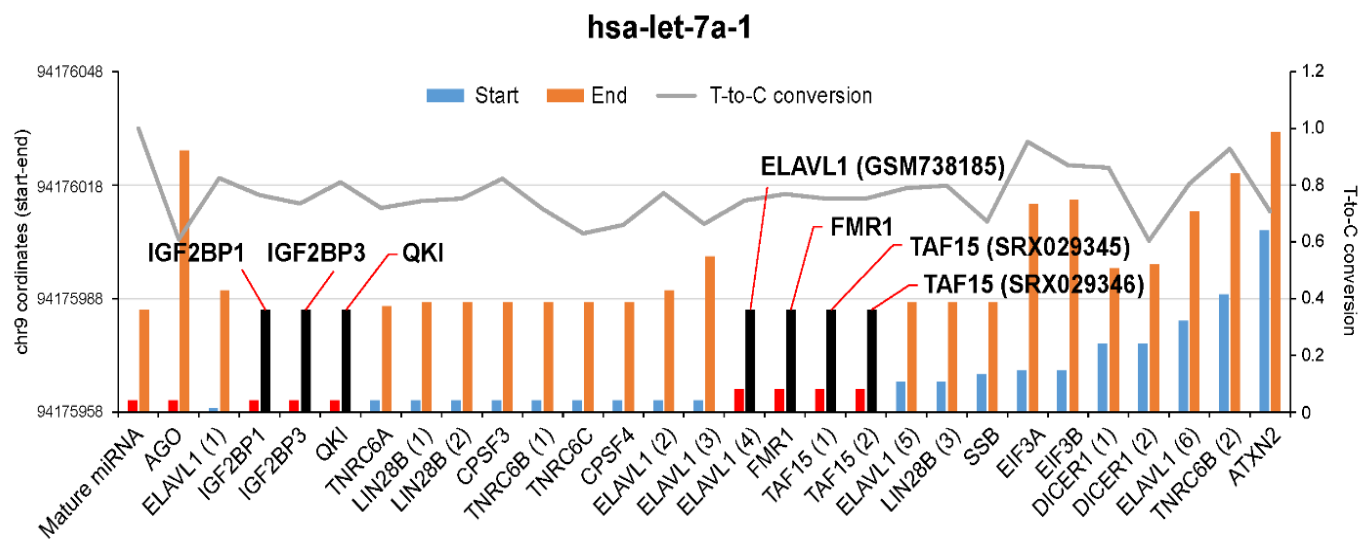
848
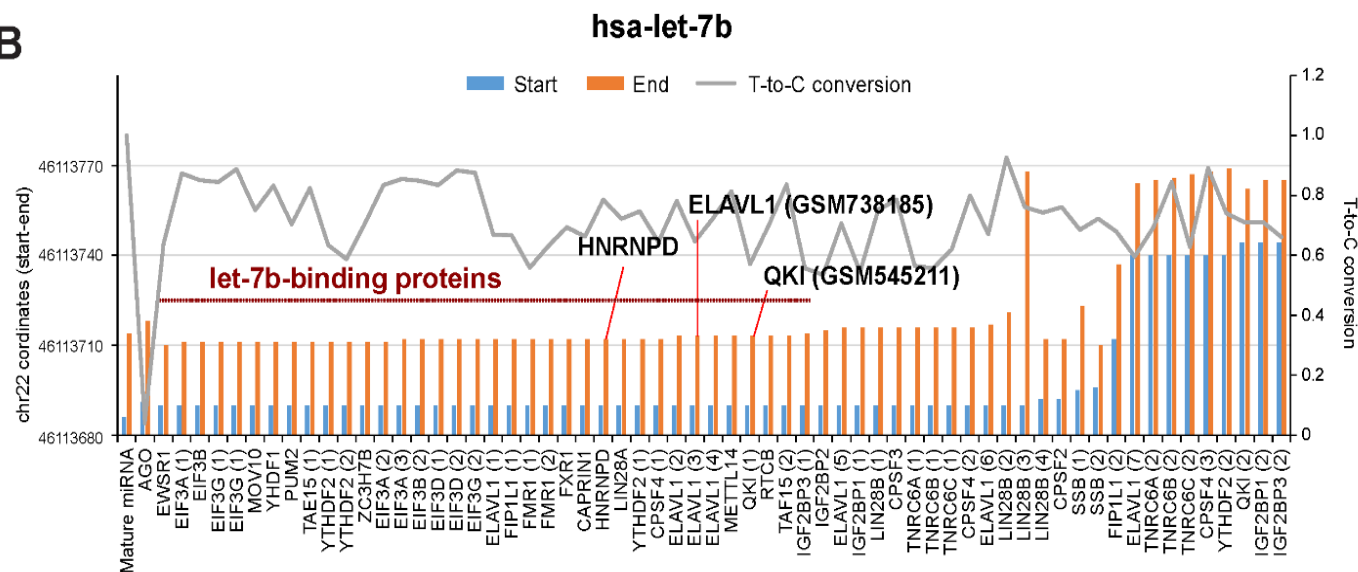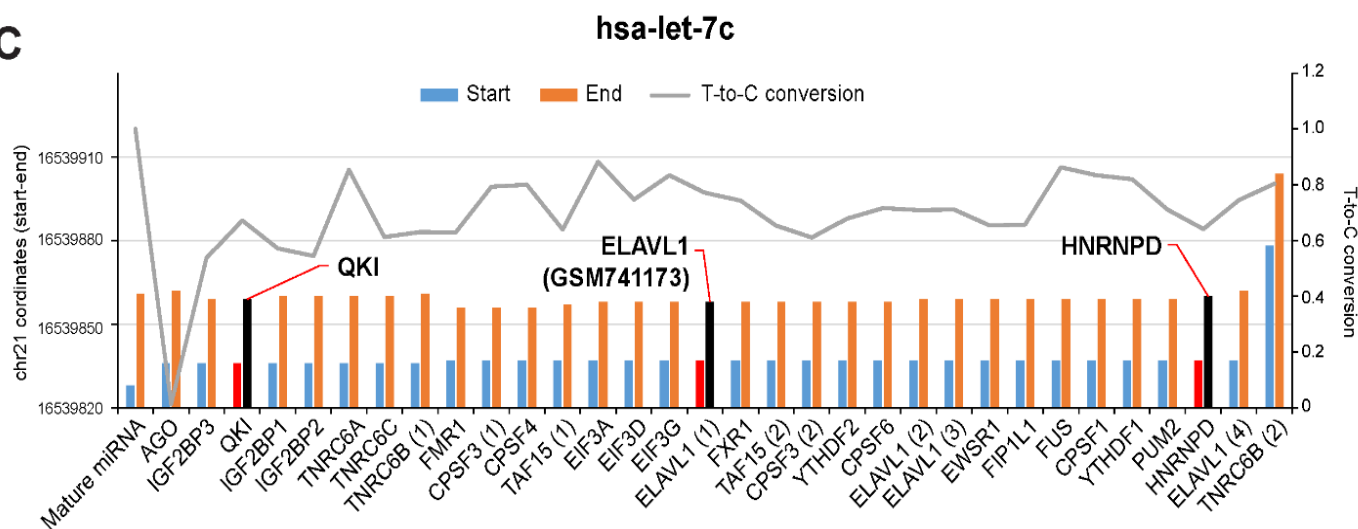
Figure 1. PAR-CLIP analysis identified RNA-binding proteins directly binding with mature and precursor miRNAs.
(A - C) Genome coordinates (y-axis) of precursor and mature miRNA let-7a-1 (A), 7b (B), and 7c (C) identified from PAR-CLIP using human cell lines. T-to-C conversion ratio was presented in y-axis as well. Representative RBPs such as QKI, HuR, hnRNPD/AUF1 and IGF2BP were highlighted.
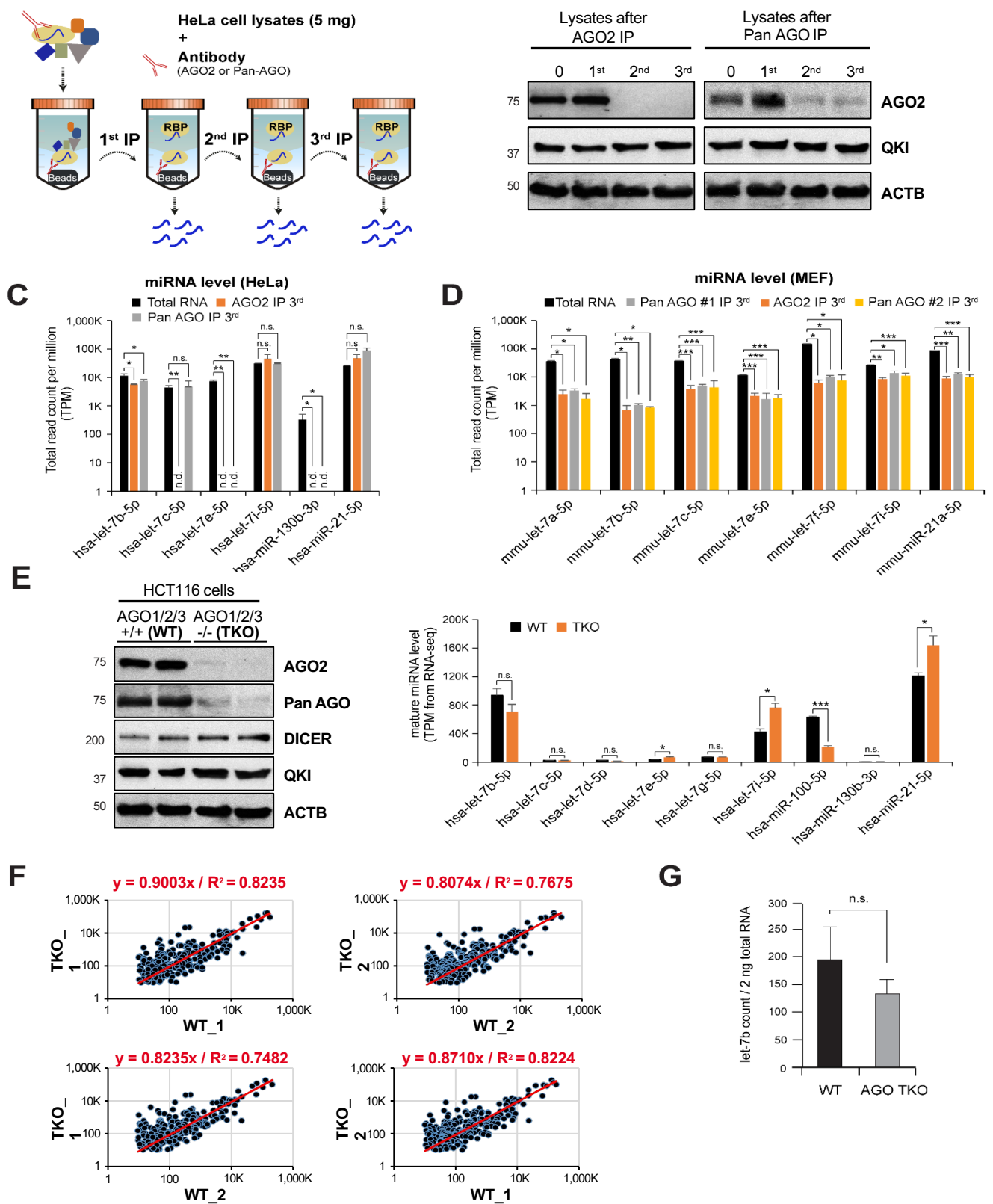
Figure 2. Existence of AGO-free mature miRNAs in human and mouse cells.
(A) Schematic of experimental set up to profile mature miRNAs from AGO-depleted human and mouse cell lysates. HeLa or MEF lysates were immunoprecipitated using anti-AGO2 or anti-Pan AGO antibodies serially. The resulting pellets and lysates were subjected to RNA purification followed by high throughput RNA-sequencing or RT-qPCR. **(B)** Western blot analysis of AGO2, QKI and ACTB using cell lysates before and after serial immunoprecipitation. **(C, D)** RNA-seq analysis of let-7, miR-21 and miR-130b using cell lysates before and after immunoprecipitation with anti-AGO2 or anti-Pan AGO antibodies. N = 2-4, n.d., not detected from RNA-seq, $***p < 0.001$, $**p < 0.01$, $*p < 0.05$, $n.s.$, not significant from Student's t-test. Data are mean ± S.D. **(E)** Western blot analysis of AGO2, Pan-AGO, DICER, QKI and ACTB using cell lysates HCT116 cells targeting AGO1, 2, and 3. RNA-seq analysis of let-7, miR-21, miR-130b, and miR-100 using HCT116 wild type and AGO TKO cells. N = 2, $***p < 0.001$, $*p < 0.05$, $n.s.$, not significant from Student's t-test. Data are mean ± S.D. **(F)** Scatter plots of miRNAs sequenced from HCT116 wild type and AGO TKO cells. **(G)** Counting of let-7b from 2 ng total RNA purified from HCT116 wild type and AGO TKO cells. N = 6, $n.s.$, not significant from Student's t-test. Data are mean ± S.D.
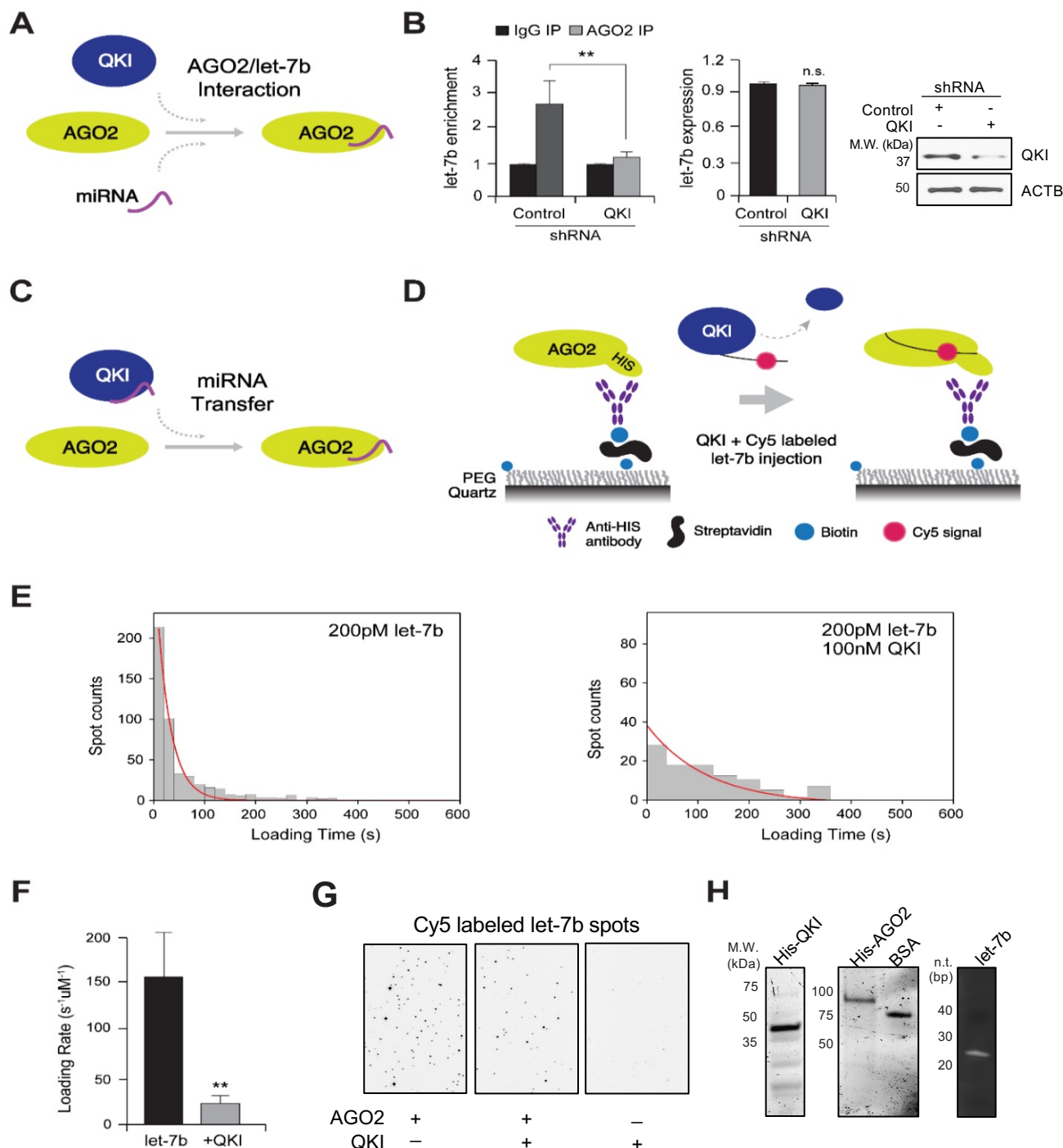
Figure 3. QKI is required for AGO2 interaction with let-7b, and allows let-7b loading onto AGO2.
(A) A model of QKI's effect on interaction of AGO2 and let-7b in human cells. (B) AGO2 RIP assay in HeLa cells after transfection of control and QKI shRNA. (*Left*) At 48 hours after transfection of shRNA targeting GFP or QKI in HeLa cells, cell lysates were subjected to immunoprecipitation against AGO2 for detection of co-purified let-7b by RT-qPCR. (*Middle*) At 48 hours after transfection of shRNA targeting GFP or QKI in HeLa cells, total RNAs were purified for detection of let-7b by RT-qPCR. (*Right*) Efficiency of QKI shRNA was determined by western blot of total cell lysates with anti-QKI or anti-ACTB antibodies. N = 3, **$p < 0.01$, *n.s.*, not significant from Student's *t*-test. Data are mean ± S.D. Data are mean ± S.D. (C) A model of QKI's effect on let-7b loading on AGO2 in single molecule analysis. (D) Single-molecule experimental scheme for let-7b (guide RNA) loading on AGO2. Recombinant AGO2 was immobilized on PEG-passivated surface using avidin-biotin interaction and anti-His tag antibody in a detection chamber. Cy5-labeled let-7b was injected into the chamber with or without QKI during the imaging. (E) Histograms of let-7b loading times in (*Left*) absence or (*Right*) presence of recombinant QKI. The red lines are single exponential decay fit (27 s and 130 s, respectively). (F) Single exponential fit was performed for loading time distributions. Loading rates of let-7b onto immobilized AGO2 with or without QKI. About 300-500 loading events were observed per experiment. N = 3, **$p < 0.01$, from Student's *t*-test. Data are mean ± S.D. (G) Cy5-labeled let-7b spots on slides with or without immobilized AGO2 and QKI 5 minutes after let-7b injection. The results of single-molecule assay. (H) Recombinant QKI and AGO2 were visualized by Coomassie Blue staining and let-7b is imaged by ethidium bromide staining. The abundance of let-7b was assessed by reverse transcriptase PCR analysis.
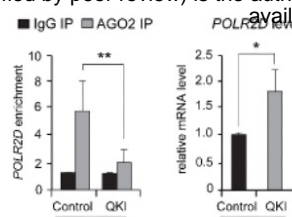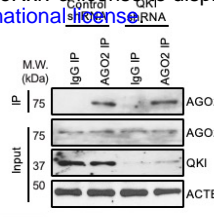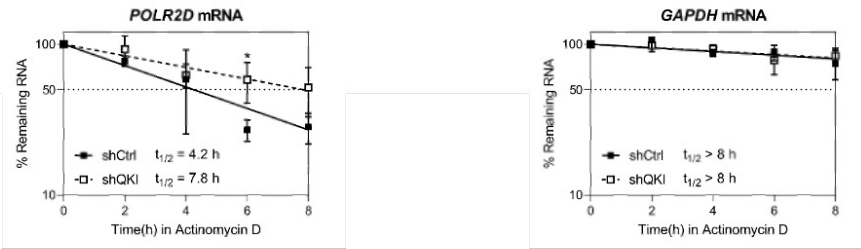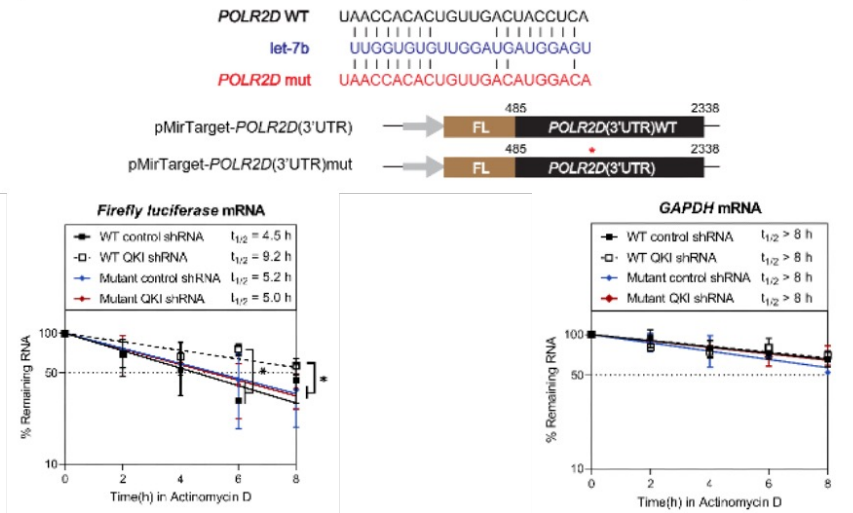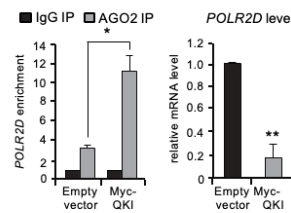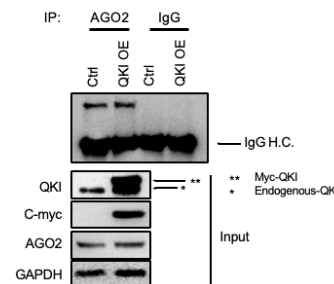
Figure 4. QKI is essential for let-7b-mediated mRNA decay.

(A) AGO2 RIP assay was performed in HeLa cells after transfection of control and QKI shRNA for detection of *POLR2D* mRNA. (*Left*) After AGO2 RIP, the amount of *POLR2D* mRNA (a let-7b target mRNA) from immune pellets were determined by reverse transcription (RT) and qPCR, with normalization to *TUBA* mRNA. (*Right*) Total RNAs were extracted from control and QKI shRNA cells for RT- qPCR. N = 3, **$p < 0.01$, *$p < 0.05$, not significant from Student's *t*-test. Data are mean ± S.D. **(B)** AGO2 RIP samples were subjected to SDS-PAGE for western blot analysis against AGO2, QKI and ACTB. **(C)** Measurement of *POLR2D* and *GAPDH* mRNA stability with Actinomycin D treatment after transfection of control or QKI shRNA in HeLa cells. At a given time of Actinomycin D treatment, total RNA was purified and converted into cDNA for quantitation of *POLR2D*, *GAPDH* mRNA, or *18S* RNA. The stability of (*Left*) *POLR2D* and (*Right*) *GAPDH* mRNAs were determined by comparing the remaining amounts of mRNA to the pre-treatment levels, which were normalized using 18S RNA. N = 3, *$p < 0.05$, *n.s.*, not significant from Student's *t*-test. Data are mean ± S.D. **(D)** Measurement of *LUC2* reporter and *GAPDH* mRNA stability after transfection of control and QKI shRNA in HeLa cells. After treatment of Actinomycin D, stability of *LUC2 (Left)* and *GAPDH* mRNAs (*Right*) were assessed by RT-qPCR with normalization of *18S* RNA (WT QKI shRNA vs WT control/mutant control/mutant QKI). N = 3, *$p < 0.05$, *n.s.*, from Student's *t*-test. Data are mean ± S.D. **(E)** AGO2 RIP assay using lysates from HeLa cells after transfection of empty vector and Myc-QKI overexpression plasmids for detection of *POLR2D* mRNA. (*Left*) After AGO2 RIP, the amount of *POLR2D* mRNA from immune pellets were determined by RT-qPCR with normalization to *TUBA* mRNA. (*Right*) Steady-state level of *POLR2D* mRNA was measured by RT-qPCR using total RNAs extracted from control and QKI shRNA. N = 3, **$p < 0.01$, *$p < 0.05$, from Student's *t*-test. Data are mean ± S.D. **(F)** AGO2 IP efficiency was verified after AGO2 immunoprecipitation and western blot analysis using lysates from HeLa cells transfected with control or Myc-QKI plasmids.
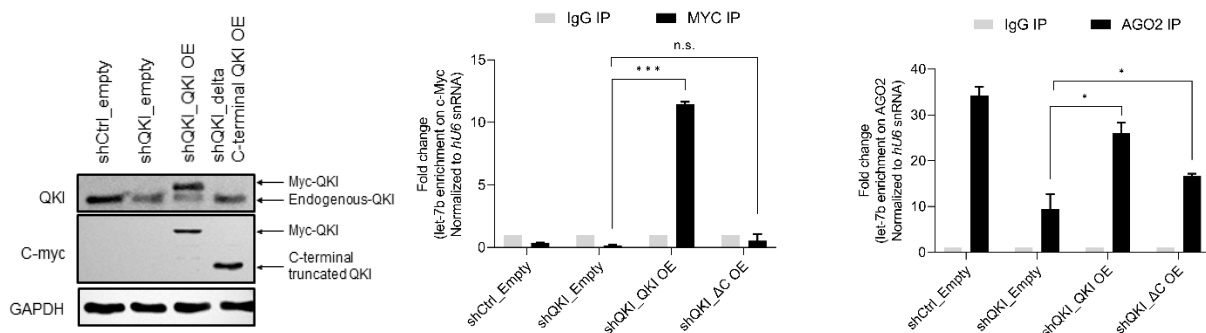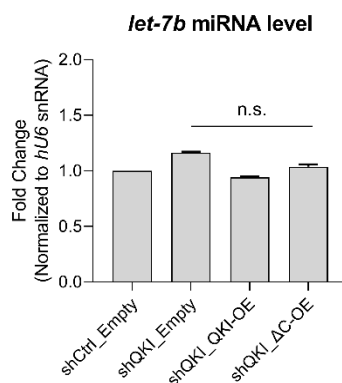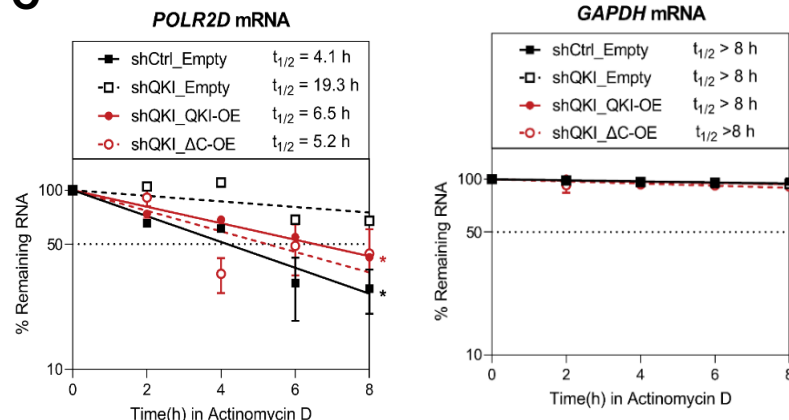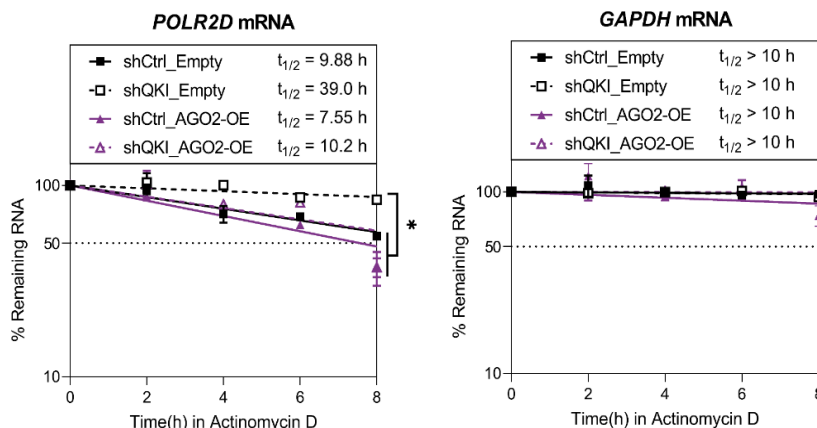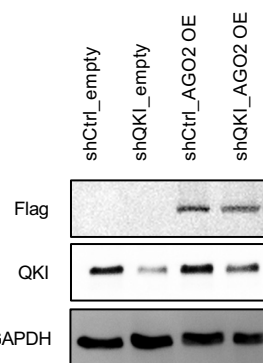
Figure 5. C-terminal region of QKI is essential for AGO2-mediated mRNA decay.
(A) (*Left*) AGO2 RIP samples were subjected to SDS-PAGE for western blot analysis against QKI, c-Myc and GAPDH. (*Middle*) MYC RIP and (*Right*) AGO2 RIP and let-7b RT-qPCR assay were performed in HeLa cells transfected with control shRNA or QKI shRNA in combination with QKI full length or CK mutant plasmids. At 48 hours after transfection, cell lysates were subjected to immunoprecipitation against AGO2 for enrichment of co-purified let-7b by RT-qPCR. N = 2, ***p < 0.001, *p < 0.05, *n.s.*, not significant from Student's *t*-test. Data are mean ± S.D. **(B)** RT-qPCR levels of let-7b using RNAs purified from the corresponding samples. N = 2, *n.s.*, not significant from Student's *t*-test. Data are mean ± S.D. **(C)** Measurement of *POLR2D* mRNA (*Left*) and *GAPDH* mRNA stability (*Right*) after re-introducing QKI full length or CK mutant in QKI knockdown cells. After treatment of Actinomycin D, stability of *POLR2D* and *GAPDH* mRNAs were assessed by RT-qPCR with normalization of *18S* RNA. N = 2, *p < 0.05, *n.s.*, from Student's *t*-test. Data are mean ± S.D. **(D)** Measurement of *POLD2D* mRNA (*Left*) and *GAPDH* mRNA (*Right*) stability after transfection of Flag-tagged AGO2 expression or empty vector in HeLa cells either stably expressing control shRNA or QKI shRNA. After treatment of Actinomycin D, stability of *POLR2D* and *GAPDH* mRNAs were assessed by RT-qPCR with normalization of *18S* RNA. N = 2, *p < 0.05, *n.s.*, not significant from Student's *t*-test. Data are mean ± S.D. **(E)** *POLR2D* mRNA stability assay samples were subjected to SDS-PAGE for western blot analysis against Flag, QKI and GAPDH antibodies.

Figure 6. QKI slows down AGO2-let-7b-target RNA assembly, and suppresses let-7b release.
(A) Detection of let-7b released from recombinant AGO2 *in vitro*. AGO2 in complex with let-7b was immobilized on the sepharose beads for detection of let-7b from the supernatant, in the presence of GST or QKI using RT-qPCR. N = 3, *$p < 0.05$, from Student's *t*-test. Data are mean ± S.D. **(B)** Detection of let-7b and *POLR2D* mRNA released from AGO2 *in vivo*. AGO2 in complex with let-7b and *POLR2D* mRNA was immobilized on the sepharose beads using HeLa cell lysates for detection of let-7b from the supernatant, in the presence of GST or QKI using RT-qPCR. N = 3, **$p < 0.01$, from Student's *t*-test. Data are mean ± S.D. **(C)** Target RNA sequence of *POLR2D* 3' UTR fragment containing let-7b site. Cy3 was labeled at the 5'-end and biotin was labeled at the 3'-end. **(D)** Single-molecule assay of RISC assembly with target RNA in the presence of QKI. The RISC solution (AGO2 and let-7b) was injected into the chamber in the presence or absence of excessive QKI (100 nM) with pre-incubation for 5 minutes. **(E)** Representative time trace of fluorescence of Cy3 on *POLR2D* fragment. The RISC solution was injected into the chamber at 40 s (dashed line). **(F)** The binding rate of let-7b to *POLR2D* target was obtained through single exponential fit of the binding time histogram. The number of data is > 330 each. N = 3, *$p < 0.05$, *n.s.*, not significant from Student's *t*-test. Data are mean ± S.D. **(G, H)** Histograms of binding time in (G) absence or (H) presence of recombinant OKI. The red lines are single exponential decay fit (17 s and 70 s, respectively), N = 3.

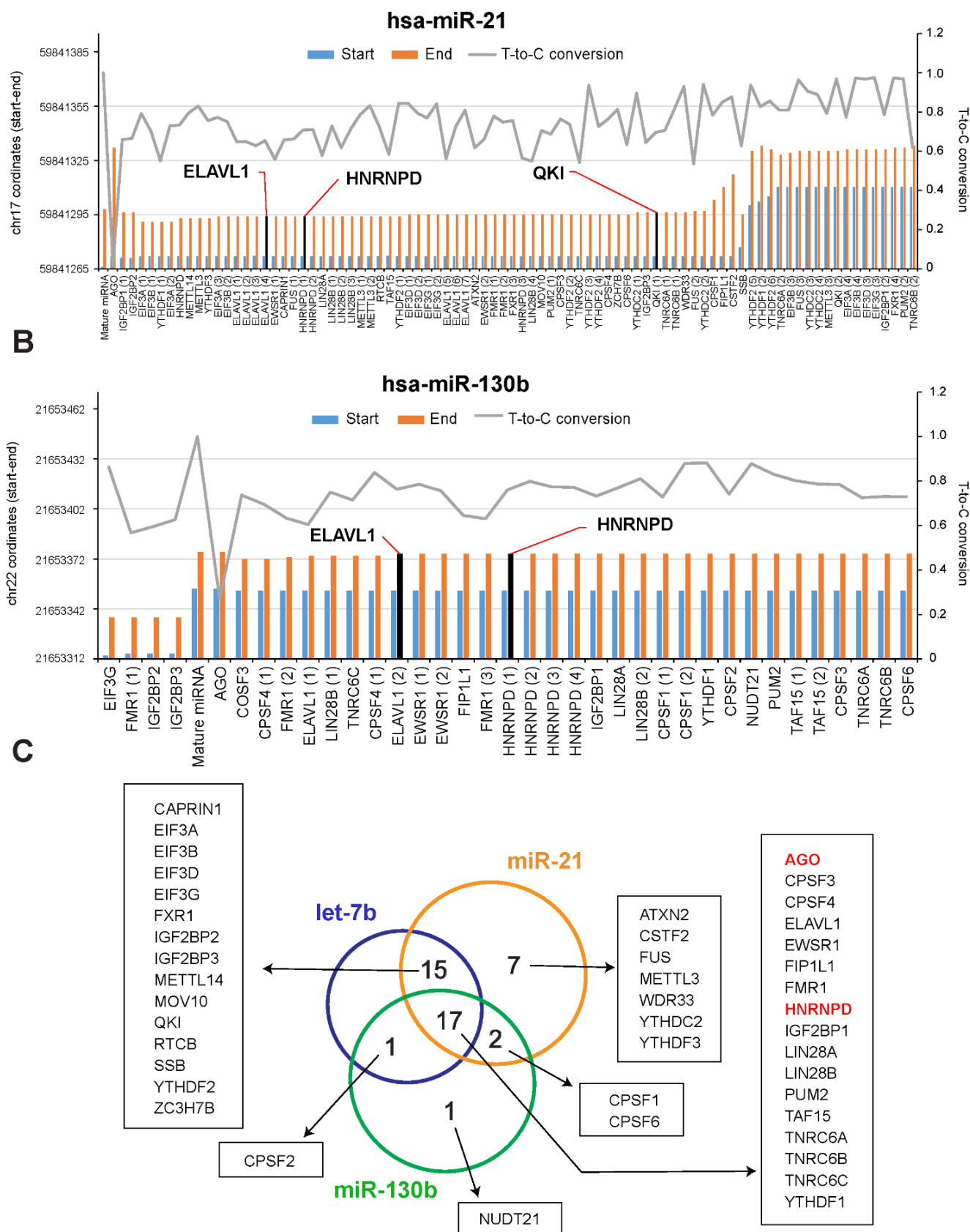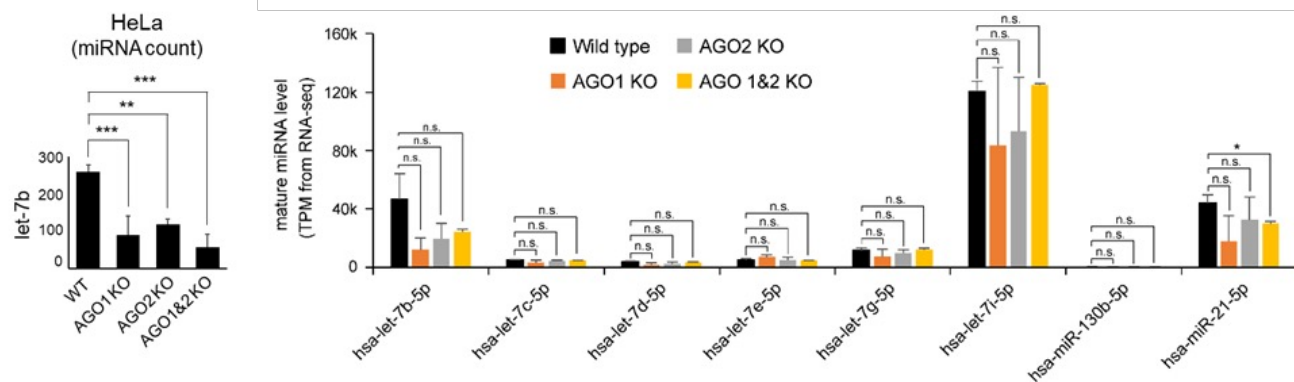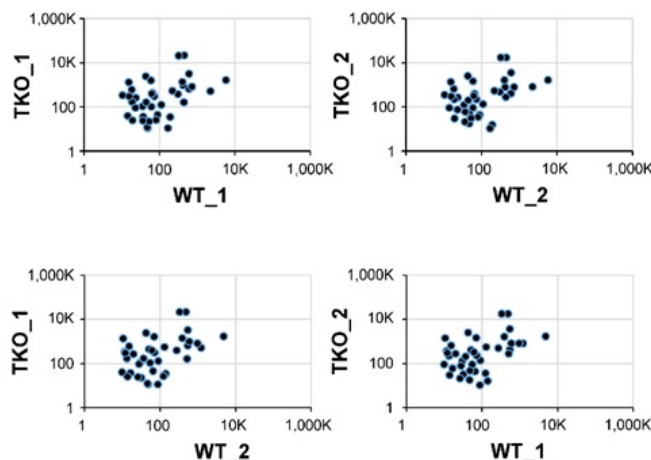**Figure S1. PAR-CLIP analysis identified RNA-biding proteins directly binding with mature and precursor let-7.**
(A, B) Genome coordinates (y-axis) of precursor and mature miRNA let-7a-2 (A, *Left*), 7a-3 (A, *Right*), and 7d (B) identified from PAR-CLIP using human cell lines. T-to-C conversion ratio was presented in y-axis as well. Representative RBPs such as QKI and HuR were highlighted. **(C)** Venn diagram 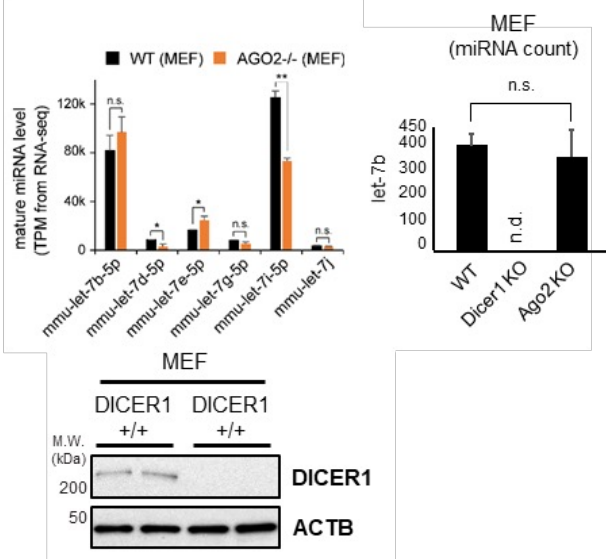of common RBPs directly binding with let-7a, 7b, 7c, and 7d. **(D)** We analyzed human QKI PAR-CLIP by sorting miRNAs in the order of T-to-C conversion counts: the top 20 miRNAs are listed.

Figure S2. PAR-CLIP analysis identified RNA-biding proteins directly binding with mature and precursor miR-21 and miR-130b.
(A, B) Genome coordinates (y-axis) of precursor and mature miRNA miR-21 (*Top*) and miR-130b (*Bottom*) identified from PAR-CLIP using human cell lines. T-to-C conversion ratio was presented in y-axis as well. Representative RBPs such as QKI, HuR and hnRNPD/AUF1 were highlighted. **(C)** Venn diagram of common RBPs directly binding with let-7b, miR-21, and miR-130b.

Figure S3. Assay of mature miRNAs when AGOs are depleted.
(A) Level of let-7b was measured by miRNA counting (*Left*) and mature miRNA let-7, miR-130b and miR-21 levels were measured by RNA-seq (*Right*) using RNAs purified from wild type, AGO1 (Talen) KO, AGO2 (Talen) KO, or AGO1/2 DKO (Talen/CRISPR) HeLa cells. N = 2, *$p < 0.05$, n.s., not significant from Student's t-test. Data are mean ± S.D. **(B)** Scatter plots of passenger strand miRNAs from RNA-seq of HCT116 wild type and AGO TKO cells. **(C)** Levels of let-7 miRNAs were measured by RNA-seq (*Left*) and by miRNA counting (*Right*) using wild type, Dicer1 KO or Ago2 KO MEFs. (*Bottom*) Western blot analysis of Dicer1 and ACTB using MEF lysates. n.d., not detected from RNA-seq, **$p < 0.01$, *$p < 0.05$, n.s., not significant from Student's t-test. Data are mean ± S.D. **(D)** Stability of let-7b (*Left*), miR-21 (*Middle*), and miR-130b (*Right*) calculated from RT-qPCR using RNAs purified from wild type, Ago2 KO or Dicer1 KO MEFs treated with Actinomycin D at a given time point.
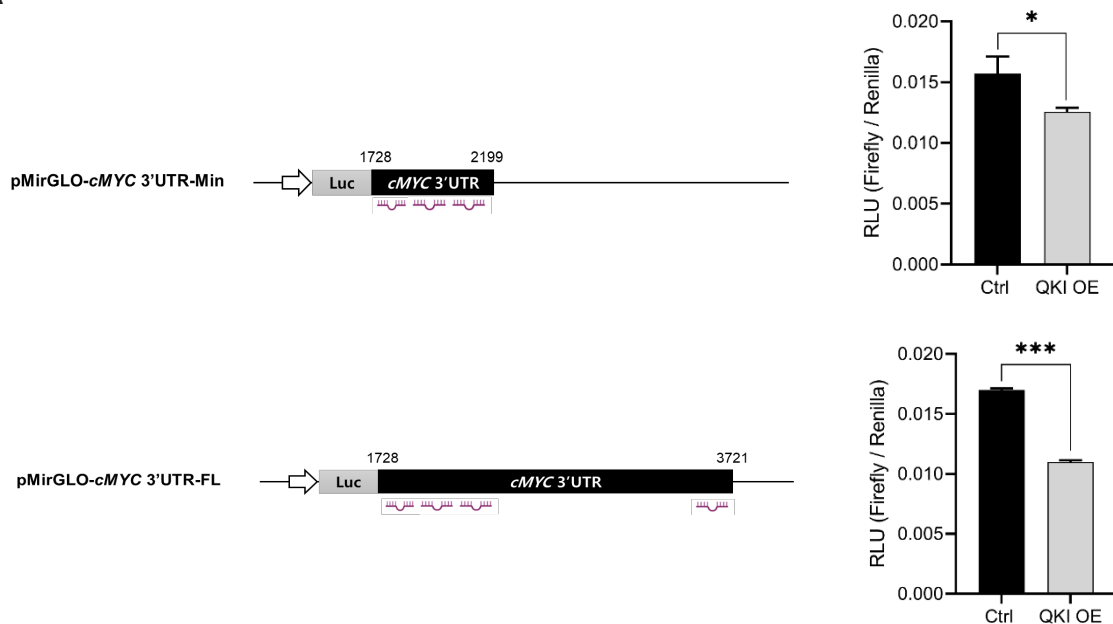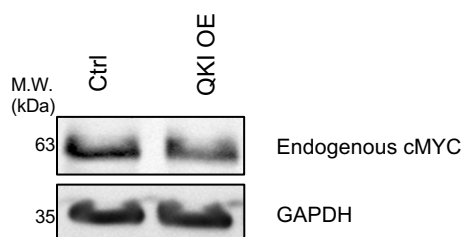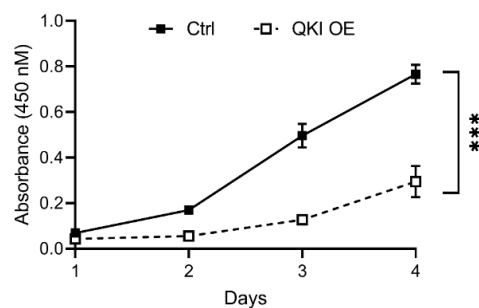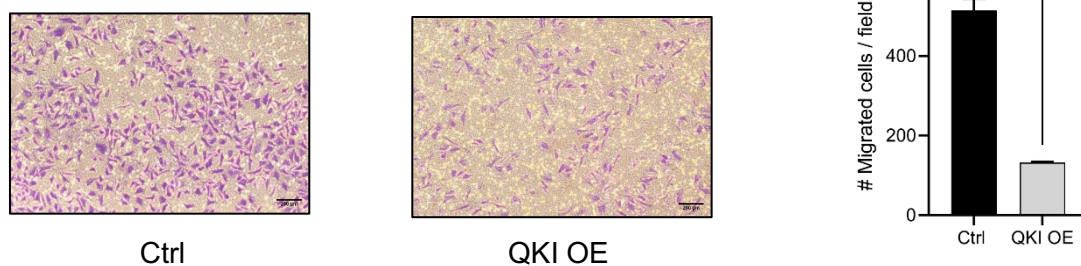
Figure S4. QKI suppresses proliferation and migration of cancer cell by enhancing 1et-7b activity.
(A) Luciferase reporter analysis for let-7b activity after transfected with QKI overexpression plasmid in HeLa cells. N = 3, ***p < 0.001*, *p < 0.05*, from Student's t-test. Data are mean ± S.D. **(B)** Western blot analyses of endogenous cMYC protein expression in HeLa cells transfected with either control or QKI overexpression plasmids. **(C)** Proliferation assay of HeLa cells that transfected with QKI overexpression plasmid. N = 4, ***p < 0.001*, from Student's t-test. Data are mean ± S.D. **(D)** Migration assay in HeLa cells after QKI overexpression. N = 3, ***p < 0.001*, from Student's t-test. Data are mean ± S.D.
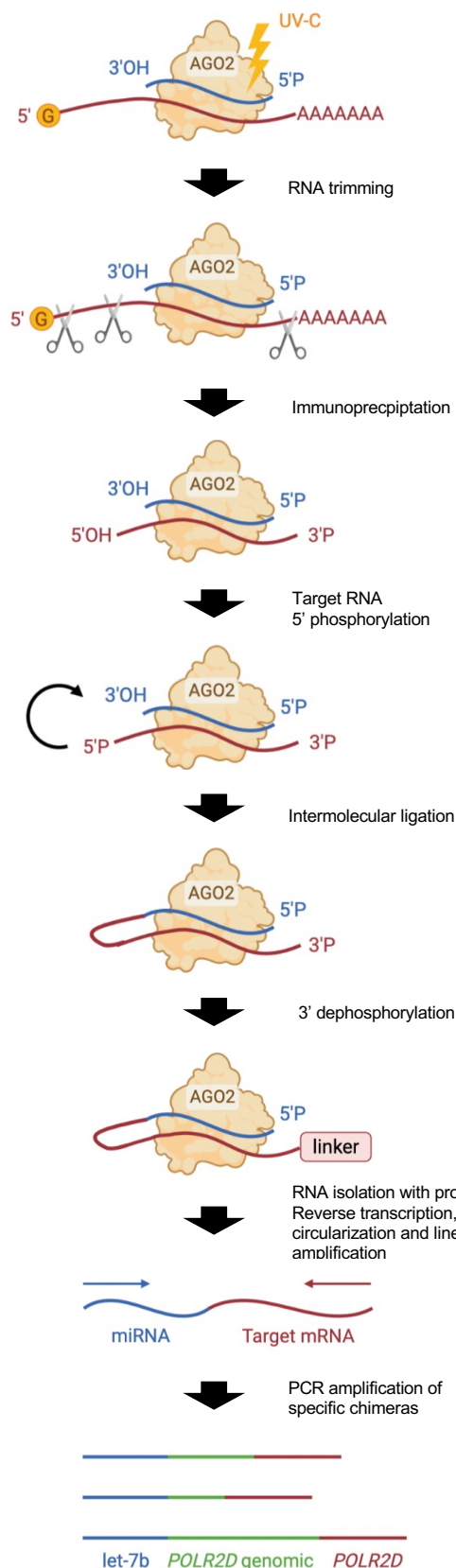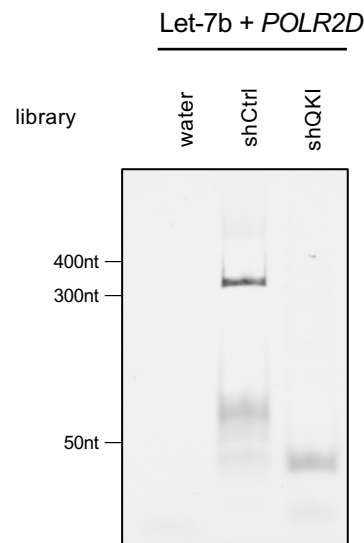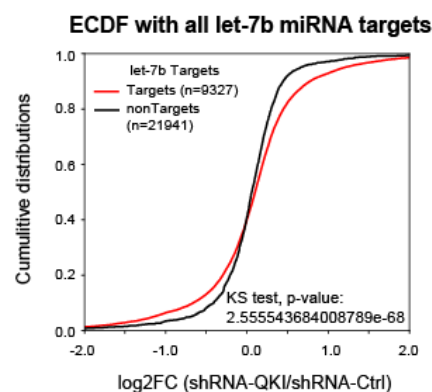
Figure S5. QKI stabilizes let-7b-POLR2D mRNA interaction.

(A) Schematic representation of the main step of Chimera PCR. **(B)** Detection of let-7b binding to the 3' UTR of POLR2D mRNA using Chimera PCR after transfection of either control or QKI shRNAs in HeLa cells. **(C)** Cumulative-distribution fraction plots (CDF) depicting the let-7b target RNAs fold change upon QKI knockdown. Significance was determined using a two-sided Kolmogorov–Smirnov (KS) test.